




Loss of Mitochondrial Localization of Human FANCG Causes Defective FANCI Helicase

Jagadeesh Chandra Bose K,^a Bishwajit Singh Kapoor,^a Kamal Mandal,^{a*} Shubhrima Ghosh,^a Raveendra B. Mokhamatam,^b Sunil K. Manna,^b  Sudit S. Mukhopadhyay^a

^aDepartment of Biotechnology, National Institute of Technology Durgapur, Durgapur, West Bengal, India

^bCenter for DNA Finger Printing and Diagnostics, Hyderabad, India

Jagadeesh Chandra Bose K and Bishwajit Singh Kapoor contributed equally to this article. Author order was determined by the order in which the first two authors worked on the study.

ABSTRACT Fanconi anemia (FA) is a unique DNA damage repair pathway. To date, 22 genes have been identified that are associated with the FA pathway. A defect in any of those genes causes genomic instability, and the patients bearing the mutation become susceptible to cancer. In our earlier work, we identified that Fanconi anemia protein G (FANCG) protects the mitochondria from oxidative stress. In this report, we have identified eight patients having a mutation (C.65G>C), which converts arginine at position 22 to proline (p.Arg22Pro) in the N terminus of FANCG. The mutant protein, hFANCGR22P, is able to repair the DNA and able to retain the monoubiquitination of FANCD2 in the FANCGR22P/FGR22P cell. However, it lost mitochondrial localization and failed to protect mitochondria from oxidative stress. Mitochondrial instability in the FANCGR22P cell causes the transcriptional downregulation of mitochondrial iron-sulfur cluster biogenesis protein frataxin (FXN) and the resulting iron deficiency of FA protein FANCI, an iron-sulfur-containing helicase involved in DNA repair.

KEYWORDS DNA damage, ICL cross-link, FANCG, FANCI, iron-sulfur cluster, mitochondria, genomic instability, DNA damage

The imbalance between DNA damage and the damage repair rate influences genomic instability, a common phenomenon and a prerequisite for cancer. The amalgamation of DNA damage by different agents (endogenous or exogenous) and lacking a DNA repair ability can augment the genomic mutation rate. It can cause the loss of heterozygosity (LOH), which in turn may activate the proto-oncogenes, deactivate the tumor suppressor gene, or both: therefore, it can act as a precursor for the deregulation of genes associated with cell cycle and cellular signals (1–3).

Under normal circumstances, when the extent of DNA damage in a cell is irreparable, these cells undergo mitochondrion-controlled apoptotic death (4), thereby precluding cellular anomaly. Oxidative radicals are the most abundant endogenous DNA-damaging agents, primarily produced by mitochondria, and studies have established the empirical relationship between the genomic instability and the overproduction of reactive oxygen species (ROS) resulting from mitochondrial dysfunction (5–7). Previous study of yeast has shown an association of mitochondrial function with genomic DNA integrity (8), whereas, recently, Ichim's group has shown that under certain conditions, mitochondrial caspase may lead to nuclear DNA damage and genomic instability (9). Therefore, the role of mitochondria in malignancy is irrefutable because mitochondria significantly act as an essential bridge between cell survival and death and are not limited to energy production and metabolism.

Several studies have reported the alteration of both the mitochondrial and nuclear

Citation K JCB, Kapoor BS, Mandal K, Ghosh S, Mokhamatam RB, Manna SK, Mukhopadhyay SS. 2020. Loss of mitochondrial localization of human FANCG causes defective FANCI helicase. *Mol Cell Biol* 40:e00306-20. <https://doi.org/10.1128/MCB.00306-20>.

Copyright © 2020 American Society for Microbiology. All Rights Reserved.

Address correspondence to Sudit S. Mukhopadhyay, sudit.mukhopadhyay@bt.nitdgp.ac.in.

* Present address: Kamal Mandal, Department of Laboratory Medicine, University of California, San Francisco, California, USA.

Received 7 July 2020

Returned for modification 11 August 2020

Accepted 17 September 2020

Accepted manuscript posted online 28 September 2020

Published 6 November 2020

genomes in different types of cancers (10–12). While the mitochondrial stability and nuclear genomic stability complement each other, the precise underlying mechanism of mitochondrion-mediated nuclear genomic stability is vaguely comprehensive. Loss of mitochondrial membrane potential causes multiple anomalies, including downregulation of iron-sulfur cluster (ISC) biogenesis, an essential mechanism for the Fe-S domain-containing proteins involved in nuclear genomic stability (13). Daniel E. Gottschling's group further substantiated the essential role of iron-sulfur cluster synthesis in genomic stability by using a specific mutant strain of *Saccharomyces cerevisiae* (3). Although the above observation is compelling with regard to mitochondrial participation in genomic integrity, the involvement of a human-pathogenic mutant study in this process will further accentuate the underlying mechanism of mitochondrion-mediated nuclear genomic stability.

In this report, we explore the hypothesis by describing the mutation of a Fanconi anemia (FA) patient cell, FA subtype G (FANCG). FA is a rare, hereditary, genomic instability and cancer susceptibility syndrome. Congenital disabilities and bone marrow failure are the prominent features of FA patients. After consecutive bone marrow transplantation (BMT), patients suffer from BMT-associated problems and undergo increased cancer risk, including hematological malignancies and head and neck cancer (14). To date, FA has 22 genes that are primarily involved in interstrand cross-link (ICL) repair, caused by exogenous alkylating agents such as mitomycin C (MMC) or endogenous metabolites such as formaldehyde and acetaldehydes (15). Upon damage, out of 22 proteins, eight (FANCA, -B, -C, -E, -F, -G, -L, and -M) form a FA core complex (16). The FA core complex formation initiates the monoubiquitination of the ID2 complex, which in turn binds the damaged part of the chromatin and, in association with other FA proteins and non-FA proteins, repairs the ICL damage via a homologous recombination pathway (16). The repair complex mostly consists of several exonucleases, endonucleases, and helicases, including FANCI.

FANCI is an ATP-dependent DEAH superfamily 2 helicase that unwinds the duplex DNA or resolves G-quadruplex DNA structures (17) and is the part of the subfamily of Fe-S cluster-containing helicase-like proteins, including XPD, RTEL1, and CHL1 (18, 19). The study of FANCI pathogenic mutation shows that the iron-sulfur (Fe-S) cluster is essential for FANCI helicase activity but not for its ATPase activity (20). FANCI cells are highly sensitive to ICL agents, and mutation studies suggest its association with cancer (21). Thus, FANCI has an essential role in ICL damage repair and in maintaining genome stability.

The earlier observation of distorted mitochondrial structure and loss of mitochondrial membrane potential in FANCG-compromised cells due to elevated ROS highlights the sensitivity of the FA cell to oxidative stress (22). Hence, many groups, including our own, have debated the role of FA proteins in mitochondria (23, 24). Our previous studies show that FA subtype G (FANCG) localizes to mitochondria and alleviates the mitochondrial oxidative stress by preventing degradation of the calpain protease-mediated mitochondrial protein peroxiredoxin 3 (PRDX3) and protects its peroxidase activity (22). This information suggests that FA proteins are involved in oxidative stress metabolism.

In this report, we have identified the N-terminal 30 amino acids, which are unique to humans, of the mitochondrial localization signal (MLS) of FANCG. Human mutation studies confirmed both the nuclear and mitochondrial roles of FANCG. The objective of the current study was to identify the defect of FANCI in FANCG mutant cells (FANCGR22P) due to oxidative stress-mediated mitochondrial dysfunction. In conclusion, we show that specific mutation in the mitochondrial localization signal of FANCG results in mitochondrial dysfunction, which thus results in genomic instability.

RESULTS

Identification of mitochondrial localization signal of human FANCG. While FA proteins are known for their role in the nuclear DNA damage repair (DDR) regulation, our earlier studies show that human FANCG (hFANCG) protein protects the mitochon-

drial peroxidase PRDX3 from calpain cleavage and eventually protects the mitochondria from oxidative stress (22). Hence, this brings up the question of how the FANCG protein migrates to mitochondria. Of the thousands of nuclear proteins that migrate to mitochondria (25), some have a mitochondrial localization signal. However, many of them do not have an identifiable signal peptide. Generally, proteins migrate to mitochondria through the interaction of TOMs (mitochondrial outer membrane protein) and TIMs (mitochondrial inner membrane protein), and some proteins enter with the help of carrier proteins (26). Human FANCG contains a tetratricopeptide repeat (TPR) motif, which is known to facilitate protein-protein interaction (27). Initially, we thought that FANCG might interact with some TPR-containing TOM proteins. However, immunoprecipitation (IP) studies did not support this idea (data not shown).

There are several online tools available for the identification of the signal peptide sequence in proteins for cellular localization, including mitochondrial localization signals (MLSs) (28). *In silico* analyses (see Table S1 and Fig. S1 in the supplemental material) confirmed our previous observation of mitochondrial localization of hFANCG (22). Specifically, iPSORT analysis identified the N-terminal 30 amino acids of hFANCG as an MLS or mitochondrial targeting peptide (mTP) (Fig. 1A). The MLS is unique in hFANCG because it is absent in other species (Fig. 1B and Table 1). Earlier, we confirmed the mitochondrial localization of hFANCG by both biochemical analyses (cellular fractionation) and cell biology (22). Here we have confirmed the *in silico* prediction of the MLS of FANCG by cell biology (expression of the protein in a mammalian cell line). Therefore, we performed the colocalization study with C-terminal enhanced green fluorescent protein (EGFP)-tagged N-terminal deletion FANCG constructs (05DEL, 09DEL, 18DEL, 24DEL, and MLSDEL [where the number in front of "DEL" represents the number of amino acids deleted and MLSDEL has 30 amino acids deleted]) containing ATG sequences as a start codon along with the mitochondrial marker MitoTracker (MitoDsRed2) (Fig. 1C). All of these deletion constructs were sequenced, and the open reading frame was confirmed. Each deletion construct, as well as a wild-type control, was transiently expressed along with MitoTracker in HeLa cells and was analyzed by a deconvolution microscope (Axio Observer.Z1 [Carl Zeiss] with Axiovision software and ImageJ). While the wild-type FANCG fused with EGFP showed perfect colocalization with MitoTracker in mitochondria of HeLa cells (Fig. 1C), the deletion constructs showed a reduction in colocalization with MitoTracker (Fig. 1C) that was ultimately lost following the deletion of 18, 24, and 30 amino acids (MLSDEL) (Fig. 1C). The scatter plot (Fig. 1C) and comparative study of Pearson's correlation coefficient (PCC) (Fig. 1D) further bolstered the microscopic colocalization study both graphically and statistically. These colocalization studies corroborate the *in silico*-predicted N-terminal 30 amino acids of FANCG as a mitochondrial targeting peptide (mTP) that determines the mitochondrial localization of human FANCG.

Human mutant FANCGR22P has lost mitochondrial localization but not nuclear localization. We further looked for pathogenic mutations in the MLS of hFANCG. We identified eight FA patients with a single-nucleotide polymorphism (SNP) of hFANCG reported in the Fanconi Anemia database of Rockefeller University (<http://www.rockefeller.edu/fanconi/>; also see the Leiden Open Source Variation Database [LOVD v.3.0] and Catalogue Of Somatic Mutations In Cancer [COSMIC] database). A single nucleotide missense mutation (C.65G>C) resulted in the conversion of arginine presented at position 22 of the MLS of hFANCG into proline (Arg22Pro). The iPSORT analysis predicted the loss of mitochondrial migration of this mutant protein (R22P) (see Fig. S2A and B in the supplemental material). During the initial structural study, the secondary structure prediction suggested that the MLS of hFANCG has an alternate stretch of coil and helix and incorporation of the mutation (C.65G>C: Arg22Pro) has resulted in the disruption of the helix (marked by a green box) due to the formation of the coil in the secondary structure of mutant FANCGR22P (marked by a red box) (Fig. 2A). Since the crystal structure of hFANCG is unknown, we modeled the tertiary structure of both wild-type hFANCG and the hFANCGR22P mutant. The modeled tertiary structure of mutant hFANCGR22P also confirmed the secondary structure

iPSORT Prediction

Predicted as: **having a mitochondrial targeting peptide**

Sequence (Type: nonplant)

```

1MSRQT TSVGS SCLDL WREKN DRLVR QAKVA QNSGL TLRRQ QLAQD ALEGL
51RGLLH SLQGL PAAVP VLPLE LTVTC NFIIIL RASLA QGFTE DQAQD IQRSL
101ERVLE TQEQQ GPRLE QGLRE LWDSV LRASC LLPDL LSAHL RLVGL QAAIW
151LSADR LGDLA LLELT LINGSQ SGASK DLLLL LKTWS PPAEE LDAPL TLQDA
201QGLKD VLLTA FAYRQ GLQEL ITGNP DKALS SLHEA ASGLC PRPVL VQVYT
251ALGSK HRKMG NPQRA LLYLV AALKE GSAWG PPLLE ASRLY QQLGD TTAEI
301ESEL LVEAL NVPCS SKAPQ FLIEV ELLLP PPDLA SPLHC GTQSQ TKHIL
351ASRLI QTGRA GDAAE HYLDL LALLL DSSEP RFSPP PSPPG PCMPE VFLEA
401AVALI QAGRA QDALT LCEEL LSRTS SLLPK MSRLLW EDARK GTKEL PYCPL
451NVSAT HLLQG QAVAQ LGAQK VAISE FSRCL ELLFR ATPPE KEQGA AFNCE
501QCKS DAALQ QLRRA ALISR GLEWV ASGQD TKALQ DFLLS VQKCP GNRDT
551YFHLL QTLKR LDRRD EATAL WLRLE AQTQG SHEDA LWSLP LYLES YLSWI
601RPSDR DAFLE EFRTS LPKSC DL
    
```

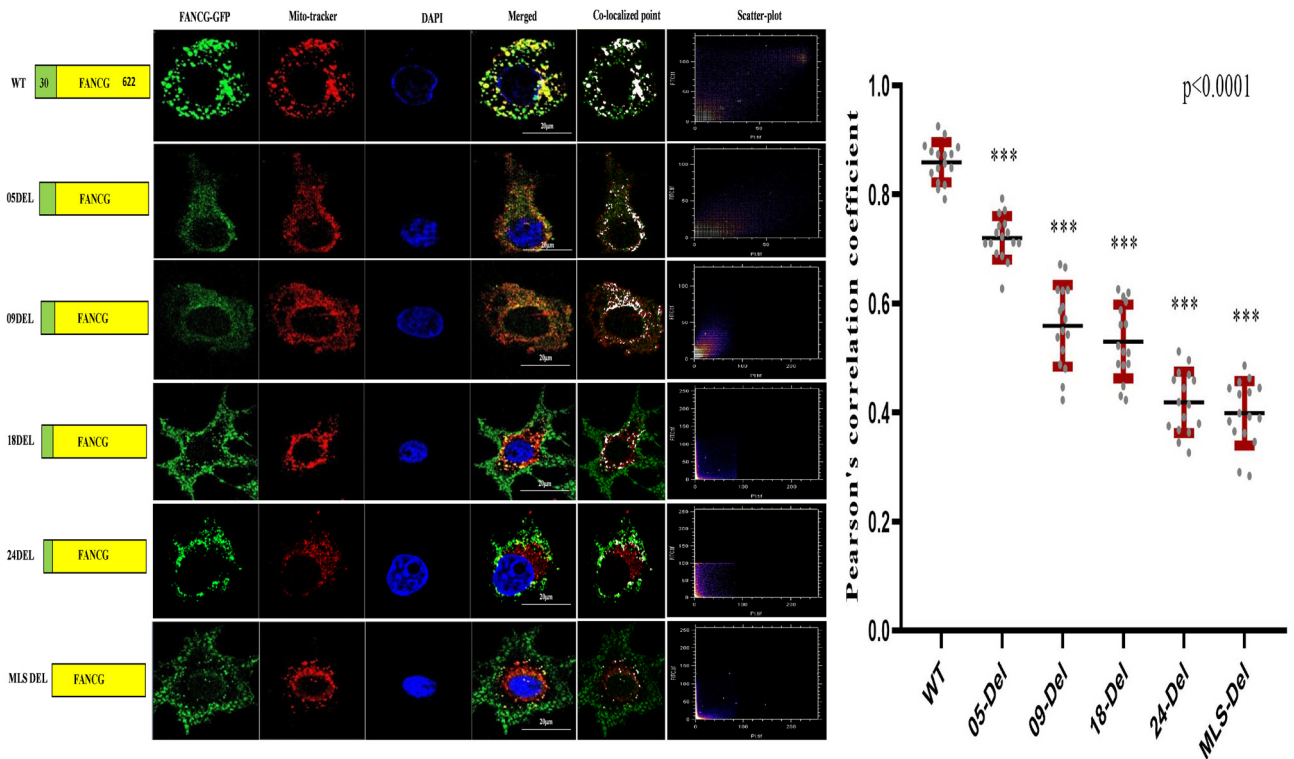
Values used for reasoning

Node	Answer	View	Substring	Value(s)	Plot
1. Signal peptide?	No	Average Hydropathy (KYTJ820101)	[6.20]	-0.6 (>= 0.953? No)	show
		Average Net Charge (KLEPS40101)	[1.30]	0.1 (>= 0.083? Yes)	show
2. Mitochondrial ?	Yes	Indexing: A11 Pattern: 221121122 (ins/del => 3)	[1.30]	MS-RQ--TTSVGSCLDLWREKNDRLVQAKVA 22-12--22220222202210000122122022 221121122	--

A

tr Q568X1 Q568X1_DANRE	MSVIPCLADRWSEENN--NIILAWKQ-NERSLQ-----	30
tr A2CE52 A2CE52_DANRE	MSVIPCLADRWSEENN--NIILAWKQ-NERSLQ-----	30
sp O15287 FANCG_HUMAN	MSR-QT-TS-VG---S--SCLDLWREKNDRLVLRQAKVA	30
tr Q53XM5 Q53XM5_HUMAN	MSR-QT-TS-VG---S--SCLDLWREKNDRLVLRQAKVA	30
sp Q9EQR6 FANCG_MOUSE	MSS-QVIPA-LPKTFS--SSLDLWREKNDQLVRQ-----	30
tr B9EJ17 B9EJ17_MOUSE	MSS-QVIPA-LPKTFS--SSLDLWREKNNQLVRQ-----	30
tr D3ZQI5 D3ZQI5_RAT	MSS-QIIPS-LPKTFS--SSLDLWREKNDQLVRQ-----	30
tr Q9EQS1 Q9EQS1_CRIGR	MSS-QIMSA-LSQTSS--STLDLWQDKNDRLVEQ-----	30
tr A7E3X0 A7E3X0_BOVIN	MAH-QT-P--LGSSASHVSCDLWREKNDQLVRQ-----	30
tr A6Y874 A6Y874_XENLA	MAG-DCLTLWMEEN-N--VIVNQWRD-SASYANTF-----	30
tr B0JZT3 B0JZT3_XENIR	MAG-DCLTLWLEEN-N--VIVSQWQG-STSCANTP-----	30
tr Q70LG7 Q70LG7_ORYLA	MNQQQSLFDYWTEENN--ELVRNCKE-GQNAVQ-----	30
tr Q7SZH6 Q7SZH6_CHICK	MKRLRC-GT-APE--P--GCLQAWAAACEALAGRWR-----	30
tr A6YGN3 A6YGN3_XENLA	MAGLPATPQSLPL--E--LSV-LYNMLIFHIHSTS---	30

B



C

D

FIG 1 Identification of the mitochondrial localization signal of human FANCG. (A) iPSort analysis of the human FANCG (highlighted sequences were predicted as MLS); (B) analysis of the conserved amino acids among the N-terminal region of the FANCG. (C) Colocalization studies of hFANCG-EGFP and MitoTracker in HeLa cells. Blue (DAPI) represents the nucleus, green represents the hFANCG-EGFP, red represents mitochondria, yellow represents the merged

(Continued on next page)

TABLE 1 Localization of FANCG in mitochondria^a

SL no.	Species name	Amino acid sequence	Entry name(s)	Gene name	iPSORT prediction for mitochondrial localization
1	<i>Homo sapiens</i> (human)	MSRQTTSVGGSSCLDLWREKNDRLVRQAKVA	C9JSE3_HUMAN	FANCG	Yes
2	<i>Mus musculus</i> (mouse)	MSSQVIPALPKTFSSSLDLWREKNDQLVRQ	FANCG_MOUSE, A4QPC9_MOUSE, Q8OX51_MOUSE, Q8VHS1_MOUSE	<i>Fancg</i>	No
3	<i>Mus musculus</i> (mouse)	MSSQVIPALPKTFSSSLDLWREKNNQLVRQ	B9EJ17_MOUSE	<i>Fancg</i>	No
4	<i>Xenopus laevis</i> (African clawed frog)	MAGDCLTLWMEENNVIWQWRDSASYANTF	A6Y874_XENLA	<i>Fancg</i>	No
5	<i>Xenopus laevis</i> (African clawed frog)	MAGLPATPQSLPELSVLNMLIFHHST	A6YGN3_XENLA	<i>Fancg</i>	No
6	<i>Xenopus tropicalis</i> (Western clawed frog)	MAGDCLTLWLEENNVIWQWRDSASYANTF	F6QKB1_XENTR	<i>Fancg</i>	No
7	<i>Cricetulus griseus</i> (Chinese hamster)	MSSQIMSALSQTSSSTLDLWKDKNDRLVEQ	Q9EQS1_CRIGR	<i>FancG</i>	No
8	<i>Rattus norvegicus</i> (rat)	MSSQIIPSLPKTFSSSLDLWREKNDQLVRQ	A0A0G2JWL4_RAT	<i>Fancg</i>	No
9	<i>Danio rerio</i> (zebrafish) (<i>Brachydanio rerio</i>)	MSVIPCLVDRWSEENNIIILAWKQNEQSLQ	Q70YH6_DANRE	<i>Fancg</i>	No
10	<i>Danio rerio</i> (zebrafish) (<i>Brachydanio rerio</i>)	MSVIPCLADRWSEENNIIILAWKQNERSLQ	A2CE52_DANRE	<i>fancg</i>	No
11	<i>Oryzias latipes</i> (Japanese rice fish)	MNQQQSLFDYWTEENNELVRNCKEQNAVQ	Q70LG7_ORYLA	<i>Fancg</i>	No
12	<i>Gallus gallus</i> (chicken)	MKRLRCGTAPGCLQAWAAECEALAGRWR	Q7SZH6_CHICK	FANCG	No
13	<i>Bos taurus</i> (bovine)	MAHQTPGLGSSASHVSLDLWREKNDQLVRQ	A7E3X0_BOVIN	FANCG	No

^aShown are N-terminal sequences of FANCG from various species, including humans, for its localization in mitochondria using the iPSORT prediction tool. Results for humans (*Homo sapiens*) are in boldface.

prediction of helix disruption compared with the wild-type hFANCG (Fig. 2B). While the structural study shows the effect of the SNP on the folding pattern of hFANCG protein, it does not vouch for the iPSORT prediction of loss of mitochondrial translocation of the hFANCGR22P mutant. Therefore, we made a C-terminal EGFP-tagged hFANCGR22P mutant construct and transiently expressed it in HeLa cells along with MitoTracker. The colocalization study suggested the complete loss of migration of R22P into mitochondria (Fig. 2C). The intensity plot shows only one co-occurrence area for hFANCGR22P and MitoTracker (marked by the black box), and the PCC value is also very close to 0 (PCC, 0.214). It further strengthens the claim of the mislocalization of hFANCGR22P into mitochondria both graphically and statistically compared with the wild-type hFANCG (PCC, 0.817) (Fig. 2C). The further extension of the colocalization study with different passages of HeLa cells as well as in FANCG knockout (KO) fibroblast cells strengthened the iPSORT prediction of the hFANCGR22P mutant's inability of mitochondrial localization (Fig. S2C and D). There were few FA patients with an SNP reported in the LOVD and COSMIC databases that causes the substitution of serine into phenylalanine (S07F) present at position 7 of FANCG. We suspected that phosphorylation of this serine might have an impact on the FANCG translocation into the mitochondria, as phosphorylation at serine 7 of FANCG plays a crucial role in the FA pathway (29, 30) that mediates the formation of BRCA2/D1-FANCD2-FANCG-XRCC3 complex (D1-D2-G-X3 complex), independent of FA core complex and D2 monoubiquitination (27). Therefore, we made the C-terminal EGFP-tagged pathogenic mutant of FANCG serine 7 (S07F) and transiently expressed it into the HeLa cells along with MitoTracker. The colocalization study showed that FANCGS07F mutant protein could localize into the mitochondria, which is further supported by the intensity plot and the PCC value (Fig. 2C). These results collectively suggest that the arginine at position 22, but not the serine at position 7, of the MLS is essential for mitochondrial localization.

FANCG, as a member of the FA core complex, remains associated with chromatin upon nuclear DNA damage, and therefore, we searched whether the mutant protein R22P can migrate to the nucleus. The cell biology studies in HeLa cells suggest that the

FIG 1 Legend (Continued)

image, and white represents the colocalized point. (D) The graph represents the Pearson's correlation coefficient for colocalization of wild-type and truncated hFANCG-EGFP and MitoTracker in HeLa cells. The values of Pearson's correlation coefficient (PCC) for colocalization of wild-type and N-terminal deletion FANCG constructs (05DEL, 09DEL, 18DEL, 24DEL, and MLSDEL) in mitochondria of HeLa cells were 0.859 ± 0.04 , 0.72 ± 0.04 , 0.559 ± 0.07 , 0.53 ± 0.07 , 0.418 ± 0.06 , and 0.398 ± 0.06 , respectively (***, $P \leq 0.0001$). For panels C and D, "WT" represents the wild type, and in 05DEL five amino acids were deleted, in 09DEL nine amino acids were deleted, in 18DEL 18 amino acids were deleted, in 24DEL 24 amino acids were deleted, and in MLSDEL the entire MLS was deleted.

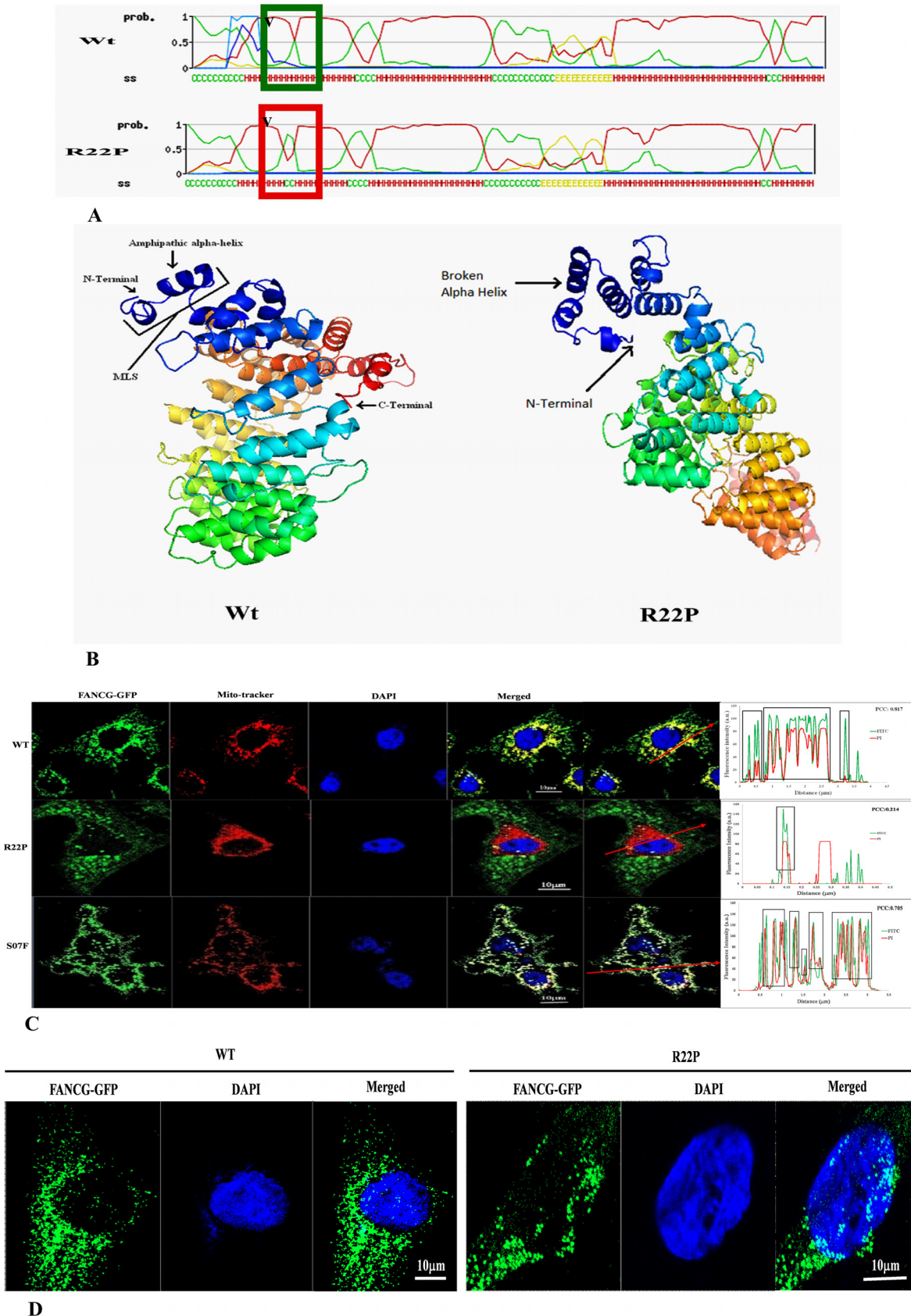


FIG 2 Localization of FANCGR22P in HeLa cells. (A and B) Secondary structure (A) and modeled 3D structure (B) of wild-type and R22P FANCG. (C) Colocalization of wild type (WT), R22P, and S07F versions of FANCG and MitoTracker in HeLa cells. The arrows represent the direction of fluorescence intensity analysis. PCC, Pearson's correlation coefficient. (D) Nuclear localization of the WT and R22P in HeLa cells treated with MMC.

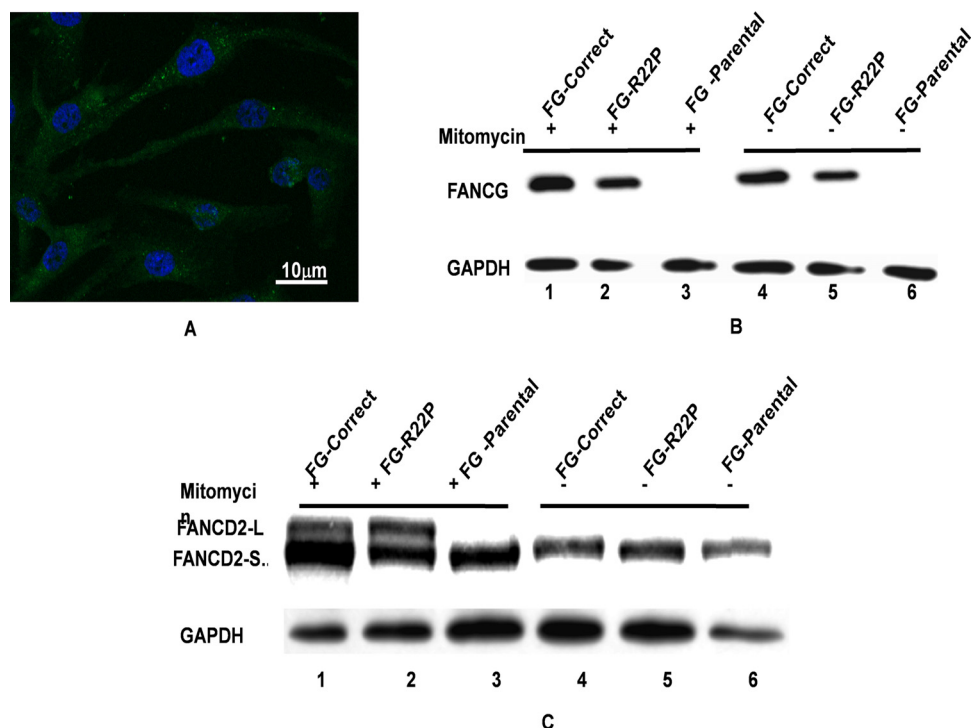


FIG 3 Development of the FANCGR22P stable cell line. The R22P construct was stably integrated into the genome of the FANCG parental cell by Lentivector pLJM1-EGFP (Addgene). (A) GFP expression confirms the stable expression of R22P in FANCG parental cells. (B) Cells were treated with MMC (lanes 1, 2, and 3) or not treated (lanes 4, 5, and 6), and cell lysates were used for Western blotting with FANCG antibody. The expression of FANCGR22P was confirmed in the stable cell (lanes 2 and 5). (C) FANCD2 monoubiquitination studies of the FANCG corrected, FGR22P, and FG parental cells. Cells were treated with MMC (lanes 1, 2, and 3) or not treated (lanes 4, 5, and 6) and blotted with FANCD2 antibody. FANCD2-L represents the monoubiquitinated proteins, and FANCD2-S represents the normal FANCD2 proteins.

mutant protein FANCGR22P could migrate to the nucleus upon MMC treatment like the wild-type FANCG (Fig. 2D). So, FANCG human mutant R22P is very unique, as it lost its mitochondrial localization but retained the nuclear localization.

FANCGR22P cells are sensitive to oxidative stress but resistant to ICL agents. In order to elucidate whether the FANCG human mutant R22P is functional in the nucleus or not, we developed an R22P stable fibroblast (FANCGR22P) cell line (see Materials and Methods) in the background of FANCG^{-/-} parental fibroblast cells (Fig. 3A and B). We performed Western blotting to examine the MMC-mediated FANCD2 monoubiquitination in the R22P stable cells, FANCG corrected cells (+/+), and in FANCG parental (-/-) cells (Fig. 3C). Surprisingly, like FANCG corrected cells, FANCD2 monoubiquitination was observed in the R22P stable cells upon MMC treatment (Fig. 3C, lanes 1 and 2), which was absent in FANCG parental cells treated with MMC (Fig. 3C, lane 3) and also in the cells not treated with MMC (Fig. 3C, lanes 4, 5, and 6). This experiment confirmed that FANCG human mutant protein R22P could participate in the formation of the FA core complex in the nucleus. In order to understand the DNA repair ability of the R22P mutant, we performed drug sensitivity tests on FANCG corrected, parental, and R22P fibroblast cells with increasing concentrations of MMC and cisplatin separately for 2 days and 5 days. Cell survival was determined using MTT [3-(4,5-dimethyl-2-thiazolyl)-2,5-diphenyl-2H-tetrazolium bromide] and the trypan blue assay (Fig. 4; see Fig. S3 in the supplemental material). To our surprise, even with 5 days of treatment with drugs at increasing concentrations, the R22P stable cells showed resistance to both MMC and cisplatin, like the FANCG corrected cells (Fig. 4A to D), and these results were also valid for formaldehyde treatment for 2 h (Fig. 4G; Fig. S3G). These drug sensitivity results suggested that FANCG human mutant protein R22P can form the FA core complex and can repair the ICL damage.

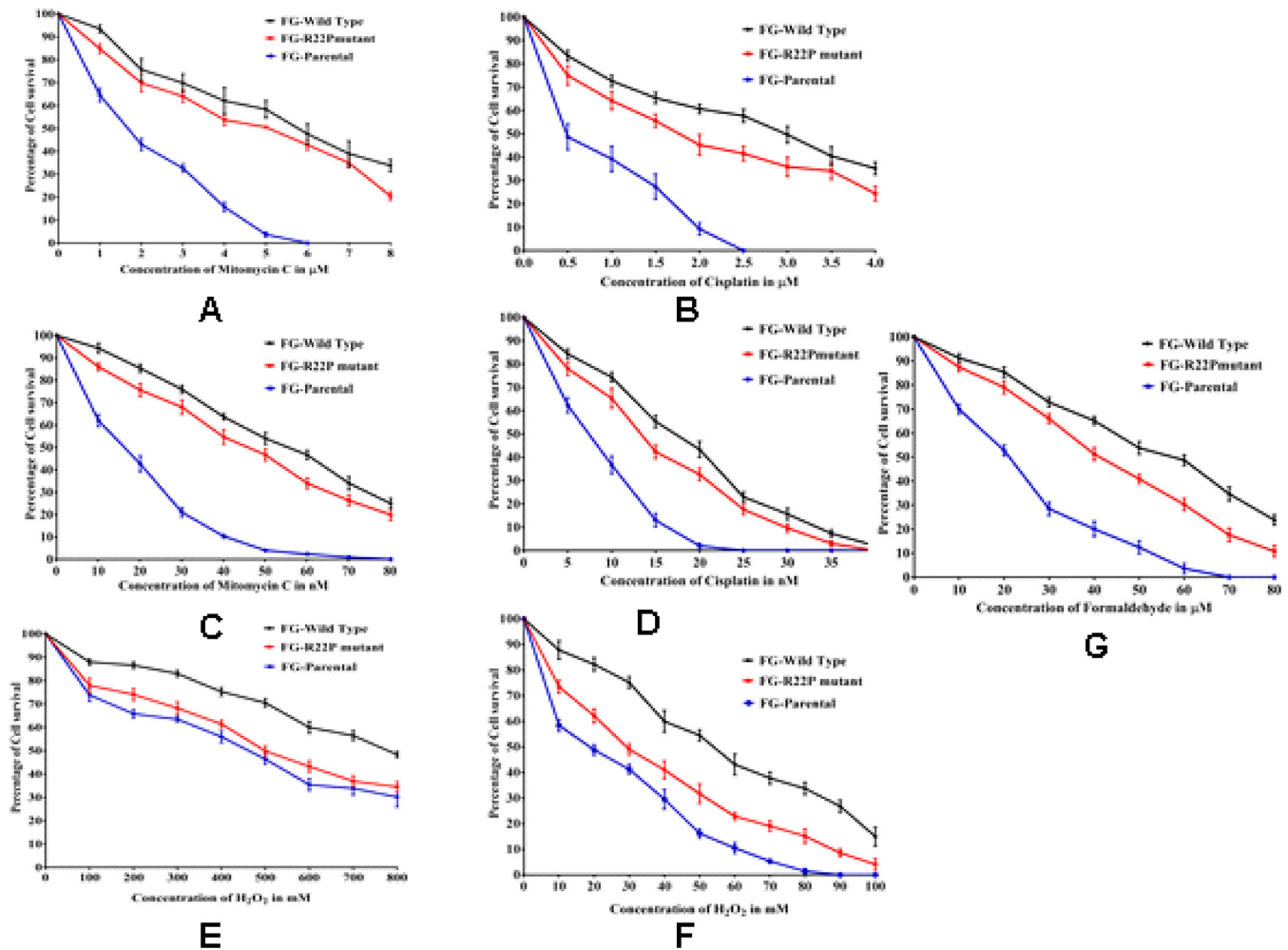
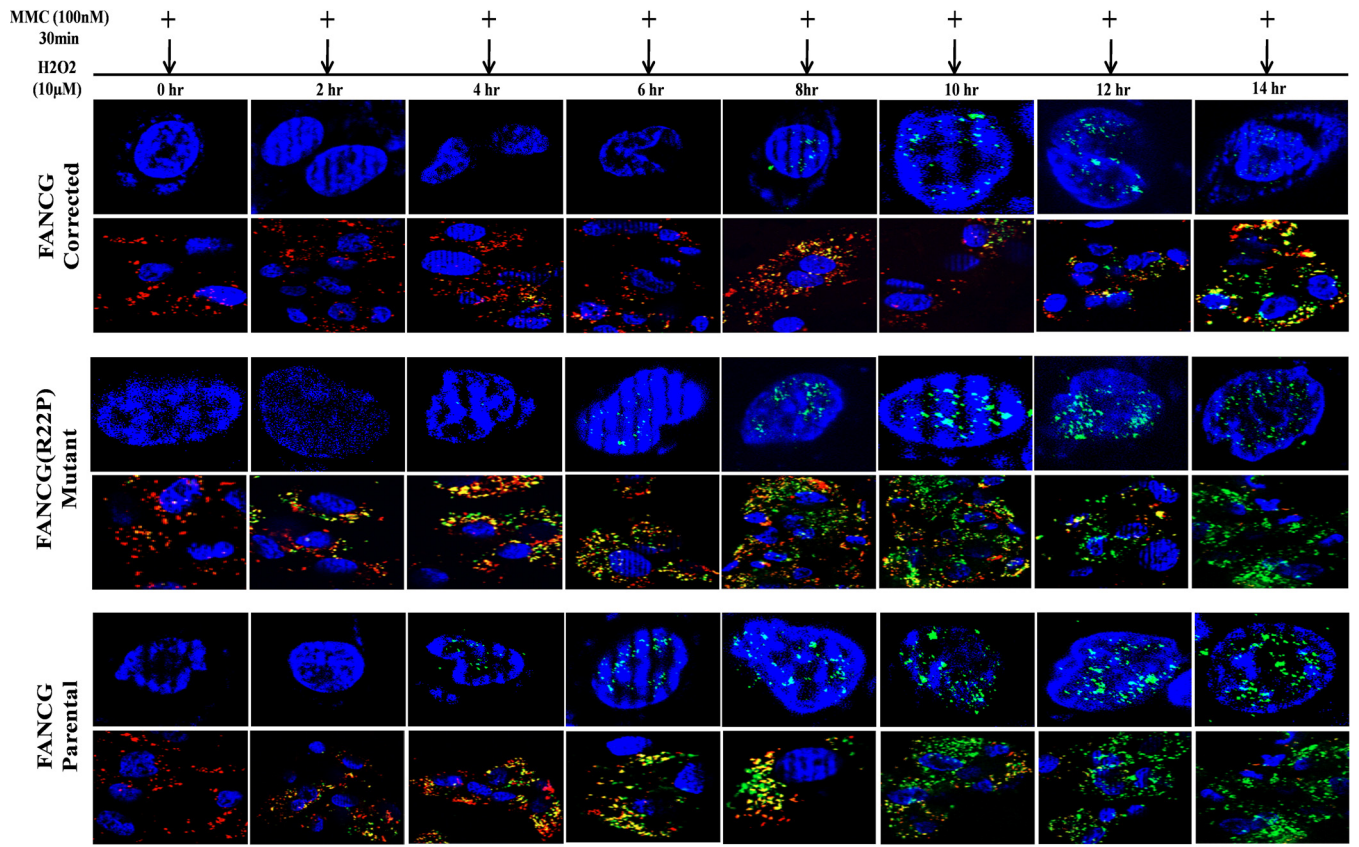


FIG 4 Drug sensitivity studies of FANCG corrected (black), FANCR22P (red), and FANCG parental cells (blue). Cells were treated with increasing concentrations of drug (MMC and cisplatin) for 2 days (A and B) and 5 days (C and D), hydrogen peroxide (H_2O_2) for 2 h (E) and 24 h (F), and formaldehyde for 2 h (G). Cell survival was determined by MTT assay. Each value is the mean from three experiments.

In contrast, when the cells were treated with hydrogen peroxide for 2 h and 24 h, like FANCG parental cells, R22P cells showed sensitivity to oxidative stress (Fig. 4E and F; Fig. S3E and F). This result also confirms our previous observation (22) of FANCG protein's role in mitochondria concerning sensitivity to oxidative stress due to diminished peroxidase activity. In summary, we can conclude that FANCG has dual roles: DNA damage repair in the nucleus and oxidative stress metabolism in mitochondria.

Correlation between mitochondrial instability and genomic instability. The R22P mutant can repair the genomic DNA; however, it fails to protect the mitochondria from oxidative stress. Despite the nuclear DNA damage repair ability, FANCR22P patients are susceptible to cancer (31). Therefore, the question remains of whether oxidative stress-mediated mitochondrial dysfunction influences the genomic DNA damage or not. Mitochondria of the R22P patients are under constant (endogenous) oxidative stress since birth that increases with age. Their genomic DNA is also under constant threat by several exogenous and endogenous ICL agents. Thus, we experimented on fibroblast cell lines to determine the extent of DDR in cells expressing the R22P mutant protein. The 0-h experimental setup was the control for all the cell types. The R22P cells, FANCG corrected cells, and FANCG parental cells were treated with mild oxidative stress ($10 \mu M H_2O_2$) for 14 h (14) continuously, followed by treatment with a low dose of MMC ($100 nM$) for 30 min at an interval of every 2 h. Then the cells were stained with JC-1 dye to determine the loss of mitochondrial membrane potential ($\Delta\Psi$)



A

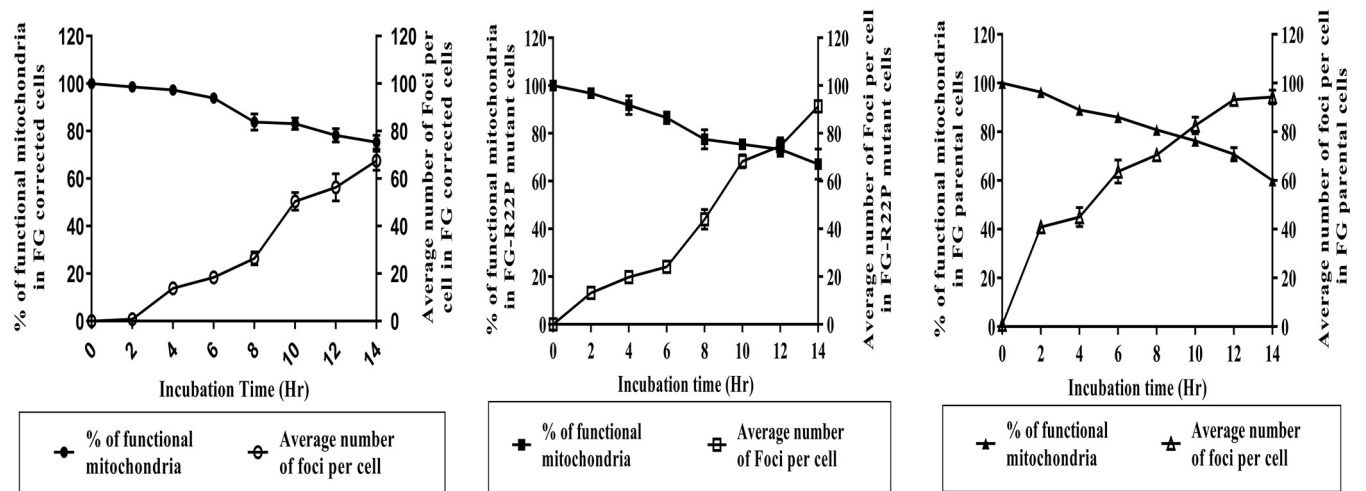


FIG 5 Mitochondrial depolarization and nuclear DNA damage in FG corrected, FG parental, and FANCD1R22P cells. Cells were treated with H₂O₂ (10 µM for 14 h) and MMC (100 nM for 30 min) at 2-h intervals. The nucleus was stained with γ-H2AX antibody, and mitochondria were stained with JC-1. (A) The green dots in the nucleus represent the γ-H2AX foci. Red represents the healthy mitochondria, green represents the depolarized mitochondria, and yellow represents the intermediate values. Arrows represent the time of MMC treatment. (B, C, and D) The graph represents the percentage of functional mitochondria and the average number of foci in FANCD1 corrected cells, FANCD1R22P cells, and FANCD1 parental cells. The values are the mean from multiple counts (more than three).

and with a specific antibody to determine the γ-H2AX focus formation in order to analyze the nuclear DNA damage (Fig. 5A). The percentages of polarized (red) and depolarized (green and yellow) mitochondria, along with the number of nuclear foci at each time point, were counted in all three types of cells. From these results, we

determined the percentage of functional mitochondria and the number of nuclear foci of the cells (8 to 10 fields, each of which contains 10 to 12 cells) as represented in graphical form (Fig. 5B to D). In FANCG corrected cells, the percentage of depolarized mitochondria was meager at initial time points (up to 6 h). From 8 h onwards, the percentage of depolarization started to increase, and by 14 h, approximately 20% of depolarized mitochondria were observed (Fig. 5B). However, in both FANCG parental and R22P stable cells, the percentage of depolarized mitochondria was very high at early time points (up to 6 h) compared to corrected cells (Fig. 5C and D), which increased with time in both cells. At 14 h, approximately 35 and 40% of mitochondria became depolarized in R22P and FANCG parental cells, respectively (Fig. 5A, C, and D). So, these experiments suggest that oxidative stress-mediated mitochondrial dysfunction is very high in FANCG parental and R22P cells compared to FANCG corrected cells.

Similarly, in FANCG corrected cells, the number of γ -H2AX foci was deficient at early time points, and then the number of foci increased with time. However, compared to the other two cells, the number of foci was low in FANCG corrected cells. At 14 h, the intensities of the foci were diminished, which suggests the intact repair ability of the FANCG corrected cells at that time point, which was not observed either in FANCG parental or R22P cells (Fig. 5A). In FANCG parental cells, the number of foci was very high at the initial time point of 2 h, and it continued to be high compared to both FANCG corrected and R22P cells (Fig. 5). The FANCG protein was absent in parental cells and, therefore, was unable to protect either the nuclear DNA or the mitochondria, whereas in R22P cells, the fact that the number of foci was lower at the initial time points of 2 to 12 h than in parental cells suggests that R22P cells can repair the DNA at early stages. After that, the numbers of foci were almost equal in both cell lines (FANCG parental and FANCG R22P) at a later stage (14 h [Fig. 5C]) due to the significant increase in mitochondrial depolarization, which crossed the apparent threshold (Fig. 5A, C, and D). All of these observations suggest that mitochondrial dysfunction influences nuclear DDR.

Mitochondrial instability causes defective FANCG in R22P cells. Nuclear genomic instability can be the result of various types of mitochondrial dysfunction (32), including the loss of mitochondrial membrane potential ($\Delta\Psi$). In yeast, mitochondrial membrane potential loss inhibits the production of iron-sulfur prosthetic groups and thereby impairs the assembly of Fe-S proteins (33), many of which act as an essential protagonist to maintain the nuclear genome (33–35).

FA subtype J (FANCG) is an essential ISC-containing helicase (18) that participates in ICL damage repair (36) to maintain genomic integrity. We attempted to observe the transcriptional downregulation of several ISC-containing proteins involved in DNA damage repair along with FANCG by real-time PCR. In our initial experiment, we did not observe transcriptional downregulation in the cells (FANCG corrected, FANCG R22P, and FANCG parental) treated with H_2O_2 (10 μM) for 14 h, followed by 30 min of MMC treatment every 2 h (data not shown).

Since the study of FANCG pathogenic mutation reinforces the salient characteristics of the iron in FANCG for its helicase activity (20), we therefore wanted to compare the status of the FANCG protein in terms of iron binding in all three sets of fibroblast cells at each time point of the experiment (10 μM H_2O_2 for 14 h, followed by 30 min of treatment with 100 nM MMC after every 2 h). Hence, we treated the cells under the condition described above in medium containing labeled iron (^{55}Fe), and after MMC treatment, we collected the cells at every time point followed by cell lysis. An equal amount of cell lysate was immunoprecipitated with FANCG antibody and protein A/G-agarose beads, followed by quantitation of ^{55}Fe to estimate the amount of iron in FANCG (37). We compared the amounts of iron present in FANCG of each cell type at different times with the amounts in their respective control counterpart cells (at zero time) considered 100 (relative percentage). The continuous reduction of iron of FANCG with time was observed only in both the R22P and FANCG parental cells (Fig. 6A). While an almost 50% loss of iron of the FANCG protein was observed in FANCG parental and

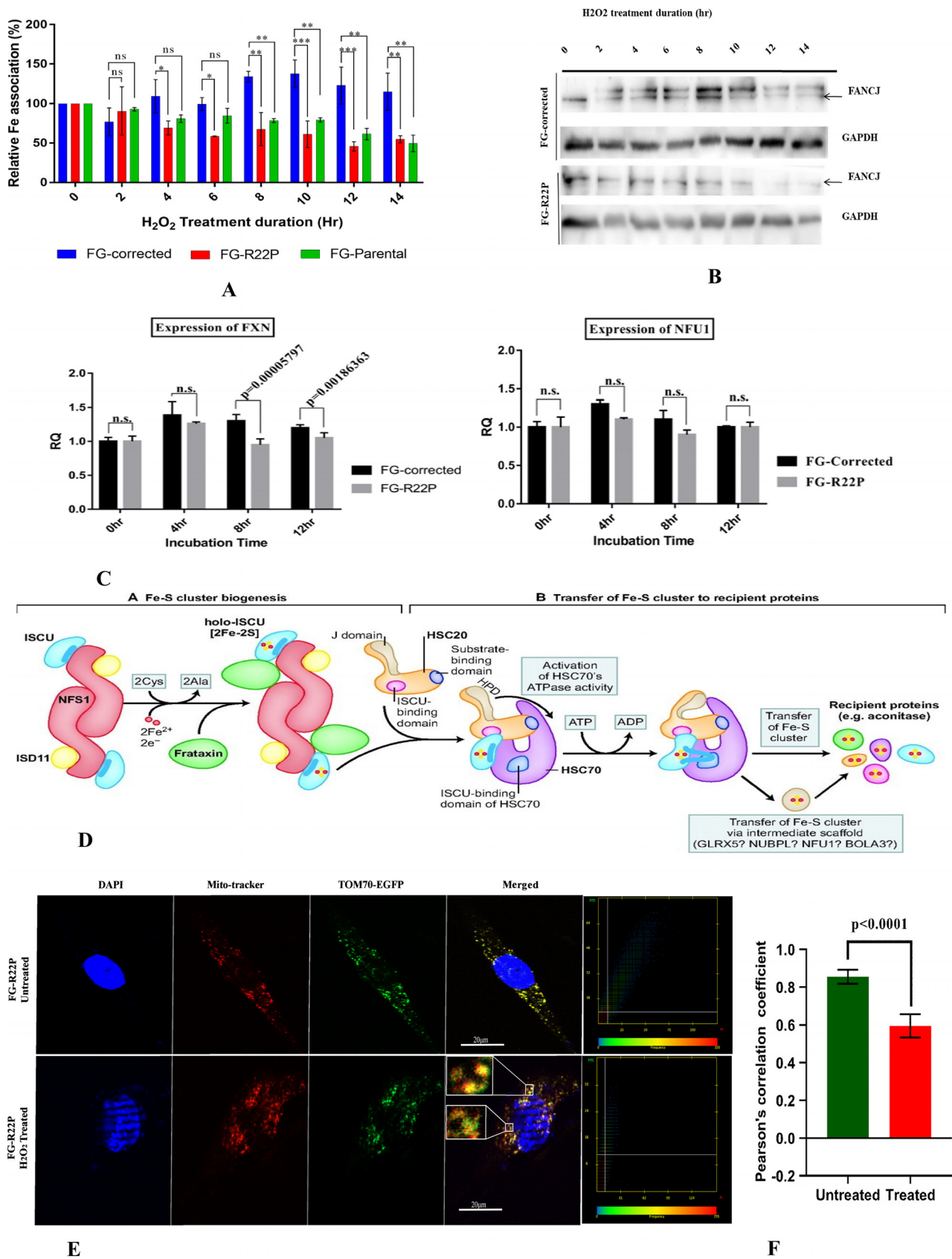


FIG 6 Quantification of the amount of iron present in FANCI protein of FG corrected, FG parental, and FGR22P cells. (A) The amount of ⁵⁵Fe at 0 h was considered 100, and the relative amount of ⁵⁵Fe was calculated at each time point. Each result is the mean from the minimum of three experiments.

(Continued on next page)

FANCGR22P cells at later stages (8, 10, 12, and 14 h) (Fig. 6A) compared to FANCG corrected cells, the percentage of iron of FANCI was unaltered or increased in FANCG corrected cells. Western blot analysis confirmed the amount of FANCI protein present in each IP (Fig. 6B). These observations suggest that loss of mitochondrial membrane potential ($\Delta\Psi$) causes iron depression of the FANCI protein only in R22P stable and FANCG parental cells. FANCI is dependent on mitochondria for the Fe-S cluster domain (18), but the iron-binding cytoplasmic protein ferritin is independent of mitochondria for the iron source (38), and loss of iron was not observed in ferritin when used as a control in these experiments (see Fig. S4 in the supplemental material). Thus, the *in vivo* iron uptake experiment suggests that the high percentage of depolarized mitochondria causes the iron deficiency of FANCI in both R22P and FANCG parental cells, which potentially affects the helicase activity.

Fe-S cluster metabolism occurs in mitochondria in two significant steps: (i) Fe-S cluster synthesis and (ii) transfer of Fe-S cluster to recipient protein (Fig. 6D). A complex of proteins is involved in each step (39). The Fe-S cluster biogenesis proteins are mainly nuclear proteins that migrate into the mitochondria. The cause of the iron deficiency of FANCI protein in R22P and FANCG parental cells could be either the difficulty in migration of the nuclear protein into mitochondria due to alteration of mitochondrial membrane potential or the downregulation of Fe-S cluster proteins due to mitochondrial stress. The translocation of mitochondrial matrix protein depends on mitochondrial membrane potential or is ATP dependent (40), whereas the localization of the TOM receptor (Tom70) utilizes preexisting TOM complexes (41) despite mitochondrial membrane potential loss (3). To help elucidate this mechanism, we transiently expressed C-terminal EGFP-tagged human Tom70 and Mito-DsRed2 MitoTracker into the R22P cells. Cells without treatment showed complete colocalization of both Tom70 and the MitoTracker; nevertheless, the cells treated with H_2O_2 did not show complete colocalization (Fig. 6E). Thus, these results indicate that the translocation of mitochondrial matrix protein depends on the mitochondrial membrane. We also studied the transcriptional expression of the Fe-S cluster genes under oxidative stress in the FANCG corrected and R22P cells. The cells were treated with $10\ \mu\text{M}\ \text{H}_2\text{O}_2$ for 12 h, followed by treatment for 30 min with $100\ \text{nM}\ \text{MMC}$ every 2 h, and we compared the levels of expression of the genes in both cells by real-time PCR (Fig. 6C).

The expression of frataxin (Fxn) was significantly decreased in R22P cells compared to FANCG corrected cells. The lower expression of FXN observed from 8 h of treatment was consistent with the result shown in Fig. 6A: FXN is essential for Fe-S cluster biogenesis. However, there was no alteration in the expression of NFX1 (Fig. 6C). NFX1 is responsible for the transportation of the Fe-S cluster to recipient proteins. Thus, these results suggest that the transcription of the FXN is significantly reduced in R22P cells compared to FANCG corrected cells because of the higher number of dysfunctional mitochondria in R22P cells. However, decreased mitochondrial migration of the ISC proteins due to loss of mitochondrial membrane potential also cannot be ruled out.

DISCUSSION

Unique mitochondrial localization signal of human FANCG. We have used different *in silico* tools to identify the mitochondrial localization signal of human FANCG. These tools predict two things: (i) whether the protein contains any mitochondrial localization signal and (ii) the mitochondrial localization of the protein. These analyses strongly predicted the N-terminal 30 amino acids of human FANCG as a mitochondrial localization signal (MLS) and correlated with the mitochondrial existence of the human FANCG. The analysis of FANCG sequences from other species suggests

FIG 6 Legend (Continued)

(ns, nonsignificant; *, $0.01 < P < 0.05$; **, $0.0001 < P < 0.0009$; and ***, $P \leq 0.0001$, for $\alpha = 0.05$). (B) Western blot of the cell lysates with FANCI and GAPDH antibody. (C) mRNA expression of FXN and NFX1 at different time points. (D) Diagram of Fe-S cluster biogenesis and transfer to recipient proteins (53). (E) Colocalization of TOM70-EGFP and the MitoTracker in FANCGR22P fibroblast cells. (F) The graph represents the Pearson's correlation coefficient for colocalization of TOM70-EGFP and the MitoTracker in FANCGR22P fibroblast cells under treated and untreated conditions.

that no species carries the MLS/mTP at either the N terminus or C terminus, except humans. Thus, one hypothesis to explain this discrepancy is that the MLS region evolved later in humans, and as a result, human FANCG has acquired the ability to regulate mitochondrial function in addition to the nuclear DNA damage repair.

Interestingly, the FANCG knockout (KO) mice do not exhibit any severe phenotype. FANCG cells derived from KO mice are only mildly sensitive to ICL agents but not sensitive to oxidative stress (42–44). However, expression studies of FANCG in other species will be required to help explain this result.

We have identified several mutations in the MLS region of human FANCG from the LOVD and COSMIC databases, and their mitochondrial localization has been studied (unpublished results). In this report, we have described one pathogenic mutation where the proline has been substituted for the arginine at position 22 (FANCGR22P). The transient expression of this pathogenic mutant fused with EGFP suggests its inability to migrate into mitochondria, whereas the mutant protein S07F (FANCGS07F) fused with EGFP showed its ability to migrate to mitochondria. This result suggests that not all point mutations in MLS affect the mitochondrial migration of FANCG. *In silico*, we have observed that mostly the mutation of the basic amino acids like lysine and arginine hampers the mitochondrial localization (data not shown). The predicted structure suggests that, as expected by many studies, the effects of proline insertions on alpha-helical structures result in broken helix due to the replacement of arginine by proline at the N terminus of FANCG. Several studies suggested the importance of arginine for mitochondrial localization of proteins (45). A most interesting feature of R22P mutant protein combines its inability to migrate to mitochondria with its ability to translocate to the nucleus. The drug sensitivity test suggests that R22P stable cells are resistant to ICL drugs like FANCG corrected cells and sensitivity to oxidative stress like FANCG parental cells.

Western blotting of FANCD2 monoubiquitination in R22P cells also suggests the ability of the mutant protein to form the FA complex. Thus, the phenotype of the R22P pathogenic mutation resolves the long-lasting debate of FA protein's role in mitochondria. Recently (2017), Zhang et al. (24) argued the role of FANCD2 in mitochondrion biosynthesis. Nevertheless, the FANCD2 monoubiquitination and its mitochondrial localization (unpublished data) in R22P cells ruled out the possibility of FANCD2 association in mitochondrial instability of R22P cells. One can raise an open question regarding the implication(s) of these results in the clinical diagnosis of FA patients. From the clinical diagnosis perspective, these results could be helpful in many patients who are diagnosed with FA by phenotypic features, although the drug sensitivity test of their cells is negative (chromosome breakage test). Hence the performance of drug test under a mild oxidative stress condition in those patients can help to reduce the diagnostic anomaly (see Fig. S5 in the supplemental material).

Mitochondrial dysfunction causes defective FANCI: mitochondrial instability leads to genomic instability. The inability of the cell to repair DNA damage may result in cancer. In this study, we have found that despite the genomic DNA repairability, the R22P patients are yet affected by cancer (LOVD database). R22P cells are highly sensitive to oxidative stress, which leads to loss of mitochondrial membrane potential (22). From these two observations, we suggest that there is a correlation between mitochondrial instability and genomic instability. Many studies suggest that mitochondrial DNA mutation and loss of mitochondrial membrane potential may cause cancer (32). One proposed mechanism is that the reactive oxygen species (ROS) produced due to mitochondrial dysfunction may destabilize the cellular macromolecules, including the damage of genomic DNA (46). So far, an association of oxidative stress with interstrand cross-linking (ICL) damage is not known. Hence, we attempted to elucidate this association by an experiment that included both oxidative damage and ICL damage in R22P cells (Fig. 5). The results suggest that R22P cells can repair the ICL damage as long as there is a certain level of functional mitochondria in the cell; below that, R22P cells fail to protect their genomic DNA from ICL damage. Fe-S-containing

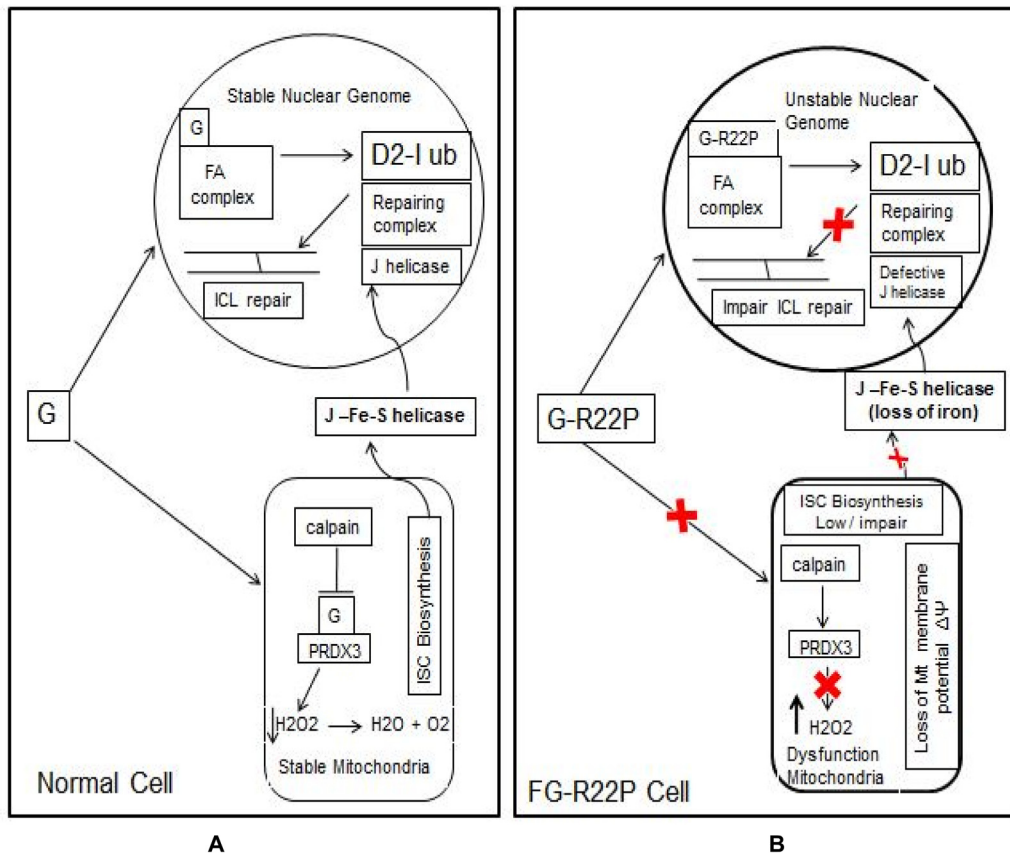


FIG 7 Model to explain the mitochondrial instability leads to genomic instability. (A) In a normal cell, FANCG prevents PRDX3 from calpain cleavage and maintains mitochondrial stability by reducing oxidative stress. Stable mitochondria maintain the helicase activity of FANCI by providing the ISC domain. (B) In the FGR22P cell, FANCG fails to migrate to mitochondria, and PRDX3 is cleaved by calpain. Mitochondrial membrane potential ($\Delta\Psi$) is lost due to elevated oxidative stress, and ISC biosynthesis is reduced. FANCI lost its helicase activity due to insufficient iron in its Fe-S domain.

proteins are essential for their role in various cellular functions such as catalysis, DNA synthesis, and DNA repair (47).

Fe-S proteins depend on mitochondria for their Fe-S domain because iron-sulfur cluster (ISC) synthesis is one of the significant functions of mitochondria (39). Several reports suggested that assembly of all ISC-containing proteins requires intact mitochondria (48). Even the loss of mitochondrial DNA or loss of mitochondrial membrane potential impairs ISC biogenesis (13). Recently, Daniel Gottschling's group has shown in a yeast system that loss of mitochondrial DNA causes a defect in mitochondrial iron metabolism (3). Nevertheless, this study is the first report of defective Fe-S-containing protein FANCI due to oxidative stress-mediated mitochondrial dysfunction. *In vivo* studies in R22P cells suggest that a significant deficiency of iron in FANCI helicase occurs due to loss of mitochondrial membrane potential (Fig. 6A). Several studies suggest that deficiency of iron of the Fe-S-containing protein may result in the loss of helicase activity (20, 49). In our studies, we have studied only FANCI, but this does not preclude the idea that other Fe-S-containing cellular proteins involved in DNA damage repair would also have affected (47). Altogether, our results strongly suggest that in healthy cells, FANCG protects the mitochondria from oxidative stress. As a result, mitochondria maintain the ISC biosynthesis and provide the Fe-S prosthetic for maintaining the Fe-S domain of active FANCI helicase, an essential element in the nuclear DNA damage repair pathway (Fig. 7). In R22P cells, ISC biosynthesis is either low or impaired due to mitochondrial dysfunction. We have identified the downregulation of FXN in R22P cells compared to FANCG corrected cells under oxidative stress conditions. FXN is an essential protein involved in ISC biogenesis, and the defect in ISC biosynthesis

leads to various human diseases. However, how the mitochondrial stress regulates the transcription of *Fxn* is not known. One possibility is via SP1, a ubiquitous transcription factor in the promoter region of the human *fxn* gene (50). The sumoylation of SP1 under oxidative stress and the subsequent lack of DNA binding have been reported (51).

The difficulty in the mitochondrial import of nuclear proteins involved in ISC biosynthesis provides another possibility. As a result, the depletion of iron or reduction in Fe-S cluster synthesis will render FANJ unable to repair the nuclear DNA (Fig. 7). We found that there is a certain percentage of defective mitochondria in the cells that does not affect the overall ISC biosynthesis in the cell. However, when this number decreases to a critical threshold, then the ISC-containing proteins will undergo an iron crisis. Further studies with R22P cells are required to identify the threshold percentage of dysfunctional mitochondria. Our studies with specific FA mutations help to confirm the relevance of the nonrespiratory function of mitochondria in disease progression, which is not unique, but a common phenomenon, the known consequence of cellular oxidative stress.

MATERIALS AND METHODS

In silico tools used. The following *in silico* tools were used: TargetP1.1 (<http://www.cbs.dtu.dk/services/TargetP/>), the iPSORT server (<http://ipsort.hgc.jp/>), MitoProt (<https://ihg.gsf.de/ihg/mitoprot.html>), PredotarMito (<https://urgi.versailles.inra.fr/predotar/predotar.html>), TPpred2.0 (<http://tppred2.biocomp.unibo.it/tppred2/default/help>), RSLpred (<http://www.imtech.res.in/raghava/rslpred/>), iLocAnimal (<http://www.jci-bioinfo.cn/iLoc-Animal>), and MultiLoc/TargetLoc (<https://abi.inf.uni-tuebingen.de/Services/MultiLoc>).

Databases used. The following databases were used: the LOVD database (<http://databases.lovd.nl/shared/variants/FANCG/unique>) and the COSMIC database (<http://cancer.sanger.ac.uk/cosmic/gene/analysis>).

Protein structure prediction. An advanced version of the PSSP server was used for the prediction of protein secondary structure by using the nearest-neighbor and neural network approach.

Tertiary structure was predicted by I-TASSER (<http://zhanglab.ccmb.med.umich.edu/I-TASSER/>). Structural templates of the proteins were first identified from the Protein Data Bank (PDB) by the multiple-threading approach LOMETS. Full-length atomic models were constructed using iterative template fragment assembly simulations. The function insights into the target proteins were finally derived by threading the three-dimensional (3D) models through the protein function database BioLiP.

Cell lines. The cell lines HeLa and HEK293 were obtained from ATCC and maintained in Dulbecco's modified Eagle's medium (DMEM) supplemented with 10% (vol/vol) fetal bovine serum (FBS) and 1× penicillin-streptomycin (Himedia). FANCG corrected (FG^{+/+}) and FANCG parental (FG^{-/-}) fibroblast cells were a generous gift from Agata Smogorzewska (The Rockefeller University, New York, NY). In contrast, FANCG mutant (R22P) fibroblast cells were prepared in our laboratory and maintained in DMEM supplemented with 15% (vol/vol) FBS and 1× penicillin-streptomycin (Himedia).

Antibodies. The following rabbit polyclonal antibodies were used: anti- γ -H2A.X (phospho-S139) antibody ab2893, anti-FANCD2 antibody ab2187, anti-DDDDK tag antibody ab1162, anti-BACH1/BRIP1 antibody ab49657, and antiferritin antibody (Sigma) F5012. The following mouse monoclonal antibodies were used: anti-FANCG antibody ab54645 and anti-GAPDH (anti-glyceraldehyde-3-phosphate dehydrogenase) antibody ab9484.

Constructs. pcDNA3-EGFP (no. 13031), pLJM1-EGFP (no. 19319), pCMV-VSV-G (no. 8454), and pSPAX2 (no. 12260) were obtained from Addgene. The construct pDsRed2-Mito, encoding a fusion of *Discosoma* sp. red fluorescent protein (DsRed2) and a mitochondrial targeting sequence of human cytochrome *c* oxidase subunit VIII (Mito), was purchased from Clontech Laboratories. Full-length FANCG wild-type (FANCG-wt) cDNA was initially cloned into TA vector pTZ57R/T (Thermo Scientific), which was further utilized as a template for the full-length and N-terminal deletion constructs of FANCG. Full-length and N-terminal deletion (up to 30 amino acids) constructs of FANCG were subcloned into the KpnI and EcoRI sites of pcDNA3-EGFP to encode C-terminal EGFP-tagged FANCG proteins. FANCG mutants were constructed by the conventional PCR method, using full-length FANCG-wt-pcDNA3-EGFP as a template, followed by DpnI treatment. FANCG mutant R22P (arginine to proline at position 22 from the N terminus) was further subcloned into the EcoRI and SpeI sites of the lentivirus vector pLJM1-EGFP. Full-length TOM70-wt was cloned into KpnI and EcoRI sites of pcDNA3-EGFP to encode C-terminal EGFP-tagged TOM70 proteins. All of the primers utilized are given in Table 2.

Immunofluorescent microscopy. Cells were grown onto poly-L-lysine-coated coverslips in 60-mm dishes and were transfected with the indicated constructs with Lipofectamine (Fermentus) for 48 h. Cells were incubated in blocking buffer (5% nonfat milk in 1× phosphate-buffered saline [PBS] plus 5% FBS in 1× PBS) for 1 h followed by a 1-h incubation with primary antibody at room temperature. After that, the cell was washed with 1× PBS followed by a 1-h incubation with the respective secondary antibody tagged with either fluorescein isothiocyanate (FITC) or Texas Red. The cells were fixed either with 4% paraformaldehyde (Himedia) for 10 min or in ice-cold methanol solution for 5 min. At 0.2%, Triton X-100 can be used as treatment for 2 min for the permeabilization of the antibody into cells. Then the coverslips

TABLE 2 Primers used for PCR amplification of FANCG truncated deletions

Name	Primer sequence ^a
05-DEL	For: 5'-CGGGATTCATGAGCTGCCTGGACCTGTGGAGGG-3'
09-DEL	For: 5'-CGGGATTCATGAATGACCGGCTCGTTCGACAGGC-3'
18-DEL	For: 5'-CGGGATTCATGCAGGCCAAGGTGGCTCAGAACTCC-3'
24-DEL	For: 5'-CGGGATTCATGGCTCAGAACTCCGGTCTGACTCTGAGG-3'
MLS-DEL	For: 5'-CGGGATTCATGCAGAACTCCGGTCTGACTCTGAGGC-3'
For all DEL ^b	Rev: 5'-GCAGAATTCCTACAGGTCACAAGACTTTGGCAGAGATGTCCG-3'
R22P	For: 5'-GGAAAAGAATGACCCGCTCGTTCGACAGG-3'
	Rev: 5'-CCTGTGCAACGAGCGGGTCAATCTTTCC-3'
TOM70	For: 5'-CGGGGTACCATGGCCGCTCTAAACCTG-3'
	Rev: 5'-CCGGAATCTAATGTTGGTGGTTTTAATCCGTATTTCTTGC-3'

^aFor, forward; Rev, reverse.

^b"For all DEL" indicates that the same primer with the reverse sequence shown was used for deletion mutants 05-DEL through MLS-DEL shown above.

were air dried and mounted with mounting medium with DAPI (4',6-diamidino-2-phenylindole [Vectashield]) on a glass slide by inverting the coverslips upside down. The mounted cells were kept in the dark for 15 min, and the coverslip was fixed with transparent nail polish. Imaging was performed on a fluorescence microscope (Axio observer.Z1; Carl Zeiss Micro-Imaging, Germany) attached to an AxioCam HRM CCD camera and Apotome.2. Axiovision software (Zenpro2012) and Adobe Photoshop 7.0 software were used for deconvolution imaging. Either Zenpro 2012 or ImageJ was used for image analysis and calculation of the Pearson correlation coefficient (PCC) for localization of two different fluorophores whose values range from +1 (perfect correlation) to -1 (perfectly negative correlation), with 0 reflecting the absence of correlation (52).

FANCGR22P mutant stable cell line development. (i) Development of virus particle in HEK293 cells. FANCGR22P was initially cloned into pCDNA3-EGFP. It was PCR cloned into the TA vector pTZ57R/T (Thermo Scientific) to create a compatible enzyme site for Lentivector (Addgene). The R22P construct was digested with EcoRI and BamHI and cloned into the viral packing vector pLJM1-EGFP (Addgene). The viral particle protein-containing vectors pCMV-VSV-G, psPAX2, and FGR22P-pLJM1-EGFP constructs were transfected (1:1:3) into HEK293 cells by Turbofect (Fermentas). The cells were grown for 48 h for the development of the virus particle.

(ii) Integration of R22P into the genome of FANCG^{-/-} parental cells. The cell culture medium containing virus particles was collected into a 15-ml sterile centrifuge tube, centrifuged at 14,000 rpm for 30 min at 4°C to remove the cellular debris, and stored at 4°C. Fresh medium was added to each HEK293 cell monolayer and incubated for another 12 h. This medium was collected, centrifuged 14,000 rpm for 30 min at 4°C, and mixed with the earlier supernatant. Total medium was filtered by a 0.22- μ m-pore syringe filter unit (Millipore) and centrifuged again for 60 min at 14,000 rpm at 4°C. Gently the supernatant was removed by pipette, fresh medium was added to the tube containing precipitate at the bottom, and again the same step was repeated to concentrate the lentivirus particles. Ultimately the supernatant containing virus was added to the flask of 60% confluent FANCG^{-/-} parental cells, and the cells were incubated for 48 h. Two days after infection, the cells were checked for GFP fluorescence, and puromycin-resistant cells were developed by adding increasing concentrations of puromycin (2 to 5 μ g/ml) to the medium. The puromycin-resistant cells were subcultured several times and preserved in freezing medium at -80°C for further usage. The stable cells were confirmed by Western blotting with FANCG-specific antibody.

Cell survival assay: cell viability test by trypan blue dye exclusion. Equal numbers of each cell type (FANCG corrected, FANCG parental, and R22P FANCG stable) were seeded into 8-well tissue culture plates with the respective blanks and controls for 24 h. DNA-damaging agents (MMC, cisplatin, H₂O₂, and formaldehyde at the concentrations described below) were added to each well and incubated for 24 h. A total of 0.1 ml of a 0.4% solution of trypan blue in the buffered isotonic salt solution (pH 7.2 to 7.3 [i.e., phosphate-buffered saline; Himedia]) was added to 1 ml of cells. These cells were loaded on a hemocytometer, and the cells were counted in each well for the number of blue-staining cells and the total number of cells. Cell viability of nearly 95% was maintained for healthy log-phase cultures. In order to calculate the number of viable cells per milliliter of culture, the following formula was used: % viable cells = $[1.00 - (\text{no. of blue cells}/\text{total no. of cells})] \times 100$, where no. of viable cells $\times 10^4 \times 1.1$ = cells/ml of culture. The viable cells were used for the preparation of the graph at each concentration of the drug. Triplicate experiments were performed for each concentration, and the data shown are the mean values from all of the results.

Cell cytotoxicity test by MTT assay. Equal numbers of cells (FANCG corrected, FANCG parental, and R22P FANCG stable) were seeded into 96-well tissue culture plates with the respective blanks and controls and incubated for 24 h. DNA-damaging agents (MMC, cisplatin, H₂O₂, and formaldehyde at the concentrations described below) were added to each well, mixed by gently rocking several times, and incubated for 48 h. A 20- μ l concentration of MTT reagent (thiazolyl blue tetrazolium bromide) at 5 mg/ml in sterile PBS (Himedia) was added to each well, mixed by gentle rocking, and incubated for 1 h. The medium was removed without disturbing the cells and purple precipitate. Dimethyl sulfoxide (DMSO [200 μ l]) was added for solubilization of the purple precipitate formazan. The plate was shaken at 150 rpm for 10 min for equal mixing of the formazan into the solvent. The optical density of the solution

was observed at 570 nm on the enzyme-linked immunosorbent assay (ELISA) plate reader. Data are the means from triplicate (minimum) experiments.

γ -H2AX focus assay. FANCG corrected (FG^{+/+}), FANCG parental (FG^{-/-}), and FANCG mutant (R22P) fibroblast cells were plated onto poly-L-lysine-coated coverslips in 60-mm dishes in DMEM with 15% (vol/vol) FBS and 1 \times penicillin-streptomycin solution and were kept in a 5% CO₂ incubator followed by serum starvation upon achieving nearly 60 to 70% confluence. These cells were treated with H₂O₂ (10 μ M) in serum-free DMEM for a continuous 14 h, followed by MMC (100 nM) treatment for 30 min in every 2-h interval. Treated cells were incubated with rabbit polyclonal anti-phospho- γ -H2AX antibody (ab11174). Goat anti-rabbit IgG-DyLight secondary antibody (Thermo Fisher) was used for 1 h, followed by DAPI staining, and foci were calculated under a microscope (Axio observer.Z1; Carl Zeiss MicroImaging, Germany) equipped with an Axiocam HRM charge-coupled device (CCD) camera and Apotome.2 Axiovision software (Zenpro 2012).

Determination of mitochondrial membrane potential loss with JC dye. The same FANCG fibroblast cells that were analyzed for γ -H2AX foci were also analyzed for mitochondrial membrane potential. At every 2 h after treatment with MMC, the cells were stained with 1 \times JC-1 dye solubilized in DMSO for 10 min. Then the coverslips were air dried and mounted with Vectashield mounting medium. The mounted cells were kept in the dark for 15 min, and the coverslip was fixed with transparent nail polish. These cells were observed under the Zeiss microscope with DAPI, FITC, and propidium iodide (PI) filters for mitochondrial membrane potential change, and deconvoluted images were captured with a fluorescence microscope (Zeiss Axio observer.Z1) fitted with an Axiocam observer camera.

The γ -H2Ax foci and the red, yellow, and green mitochondria were counted from the 8 to 10 fields, each of which contained 10 to 12 cells. The final results are presented as the mean values from all the counts.

In vivo iron uptake assay of FANCI. Fibroblast cells (FANCG corrected, FANCG parental, and R22P stable cells) were grown at 37°C with 5% CO₂ in Iscove's modified Dulbecco's medium (IMDM; Sigma) supplemented with 15% (vol/vol) FBS (Gibco) and 1 \times penicillin-streptomycin solution (Gibco) for 24 h (37). This was followed by a second incubation for 2 h in IMDM containing 15% (vol/vol) FBS, 1 \times penicillin-streptomycin, and 10 μ Ci ⁵⁵Fe (BARC, India). Following serum starvation in IMDM containing 10 μ Ci ⁵⁵Fe for 2 h, these cells were treated with H₂O₂ (10 μ M) in serum-free IMDM for a continuous 14 h, followed by MMC (100 nM) treatment for 30 min in every 2-h interval. Cells were collected, washed three times with 1 \times PBS, and lysed in IP lysis buffer (25 mM HEPES, 100 mM NaCl, 1 mM EDTA, 10% [vol/vol] glycerol, 1% [vol/vol] NP-40) supplemented with 1 mM phenylmethylsulfonyl fluoride (PMSF), 10 mM dithiothreitol (DTT), 1 mM sodium orthovanadate, 10 ng/ml leupeptin, and 1 ng/ml aprotinin. Approximately 700 μ g cell lysate was incubated with 4 to 5 μ l of IP-grade polyclonal FANCI antibody (Abcam) and ferritin antibody (Sigma) for 1 h at 4°C. Ferritin was taken as a control for iron uptake by cells. A total of 30 μ l of protein A/G plus agarose beads (Biobharti, India) was added, and the mixture was incubated at 4°C overnight under constant shaking. Beads were washed three or four times with 1 \times IP lysis buffer. Washed beads were boiled in 10% (wt/vol) SDS solution and were mixed with scintillation oil. Disintegrations per minute (dpm) of ⁵⁵Fe were counted in a liquid scintillation counter. The results shown are the mean value from triplicate experiments.

DNA substrate. Standard desalted oligonucleotides were purchased from IDT and were used for the preparation of DNA substrates. The forked-duplex DNA substrate was prepared from the DC26 and TSTEM25 oligonucleotides, as described by Wu et al. (20).

FANCI helicase assay. Fibroblast cells (FG^{+/+}, FG^{-/-}, and R22P mutants) were grown at 37°C with 5% CO₂ in DMEM (Gibco) supplemented with 15% (vol/vol) FBS (Gibco), and 1 \times penicillin-streptomycin solution (Gibco) for 24 h, followed by serum starvation in DMEM for 2 h. These cells were treated with H₂O₂ (10 μ M) in serum-free DMEM for a continuous 14 h, followed by MMC (100 nM) treatment for 30 min. In every 2-h interval, cells were collected, washed three times with 1 \times PBS, and lysed in IP lysis buffer (25 mM HEPES, 100 mM NaCl, 1 mM EDTA, 10% [vol/vol] glycerol, 1% [vol/vol] NP-40) supplemented with 1 mM PMSF, 10 mM DTT, 1 mM sodium orthovanadate, 10 ng/ml leupeptin, and 1 ng/ml aprotinin. Approximately 700 μ g cell lysate was incubated with 4 to 5 μ l of IP-grade polyclonal FANCI antibody (Abcam) for 2 h at 4°C, followed by a 3-h incubation with 30 μ l of protein A/G plus agarose beads (Biobharti, India) at 4°C under constant shaking. Beads were then collected by centrifugation at 4°C and washed two times with 1 \times IP lysis buffer and two times with 1 \times helicase buffer (40 mM Tris-HCl [pH 7.4], 25 mM KCl, 5 mM MgCl₂, 0.1 mg/ml bovine serum albumin [BSA], 2% [vol/vol] glycerol, 2 mM DTT). The helicase reaction was initiated by incubating FANCI-bound washed protein A/G plus agarose beads at 37°C for 30 min with a helicase reaction mixture containing helicase buffer and 2 mM ATP, and 0.5 nM DNA substrate was then incubated with helicase buffer and 0.5 nM DNA substrate. Reactions were terminated using stop buffer (0.3% [wt/vol] SDS and 10 mM EDTA). The reaction product was resolved on nondenaturing 11% (30:1 acrylamide-bisacrylamide) polyacrylamide gel followed by drying and then was subjected to autoradiography.

RNA isolation, cDNA synthesis, and real-time PCR. Fibroblast cells (FG^{+/+} and R22P mutants) were grown at 37°C with 5% CO₂ in DMEM (Gibco) supplemented with 15% (vol/vol) FBS (Gibco), and 1 \times penicillin-streptomycin solution (Gibco) for 24 h, followed by serum starvation in DMEM for 2 h. These cells were treated with H₂O₂ (10 μ M) in serum-free DMEM for a continuous 12 h, followed by MMC (100 nM) treatment for 30 min. At every 4-h interval, cells were collected by trypsinization. Total RNA was isolated from these harvested cells using TRIzol (Ambion, Life Technology) and then was stored at -80°C until further use.

TABLE 3 Sequences of the primers used for real-time PCR

Gene product	NCBI reference sequence	Sequence (5'→3')	Amplicon length (bp)
FXN	NM_000144.4	For: AGCCATACACGTTTGAGGACTATGA Rev: ACGCTTAGGTCCACTGGATGG	149
NFU1	NM_015700.3	For: TCCCCTCTGGCTAGGCAGTTA Rev: GCAAAGAAGTCCATGATTGTTGCAT	149
β -Actin	NM_001101.5	For: GGCCAACCGCGAGAAGAT Rev: CGTCACCGGAGTCCATCA	134

A total of 4 μ g of the total RNA isolated as described above was used to prepare cDNA using the Verso cDNA synthesis kit (Thermo Scientific), following the manufacturer's protocol. Prepared cDNA was then diluted five times, and 2 μ l of this diluted cDNA was used as a template for real-time PCR.

Real-time PCR was performed on the StepOnePlus real-time PCR system (Applied Biosystems) using the SYBR green PCR master mixture (Applied Biosystems, Thermo Fisher Scientific). The program was set as follows: a holding stage at 95°C for 10 min, a cycling stage of 40 cycles at 95°C for 15 s, 57°C for 1 min, and 60°C for 1 min, and a melting curve stage, consisting of a step and hold at 95°C for 15 s, 60°C for 1 min, and 95°C for 15 min with a ramping rate of +0.3°C. β -Actin was used as an endogenous control. The sequences of primers used for real-time PCR are given in Table 3. Graph Pad Prism 7 was used to perform multiple *t* tests to evaluate statistical significance, using the two-stage linear step-up procedure of Benjamini, Krieger, and Yekutieli, with a desired false-discovery rate (*q*) = 5%, without assuming a consistent standard deviation.

Chromosome preparation. Fibroblast cells (R22P mutants) were grown at 37°C with 5% CO₂ in DMEM (Gibco) supplemented with 15% (vol/vol) FBS (Gibco) and 1 \times penicillin-streptomycin solution (Gibco) for 24 h, followed by serum starvation in DMEM for 2 h. These cells were treated with either MMC (100 nM) or H₂O₂ (300 μ M) and MMC (100 nM) in serum-free DMEM for a continuous 2 h, followed by colcemid (200 μ g/ml) treatment for 1 h. These cells were harvested by trypsinization and were treated with KCl (75 mM) for 30 min, followed by a 10-min treatment in fixative (1 part acetic acid and 3 parts methanol). Cells were then spread on cold glass slides by the dropping method followed by a continuous flush with 1 ml fixative two times. Slides were air dried and then mounted with mounting medium containing DAPI (Vectashield). The mounted slides were kept in the dark for 15 min. Imaging was performed on a fluorescence microscope (Axio observer.Z1; Carl Zeiss Micro-Imaging, Germany) attached to an Axiocam HRM CCD camera with Apotome.2 Axiovision software (Zenpro 2012). The results were analyzed from the multiple fields of several experiments and were very consistent.

Statistical analysis. Data were analyzed with GraphPad Prism (version 8.0). Results are expressed as the mean and standard deviation (SD). The Shapiro-Wilk test was used to analyze the normal distribution of the variables (*P* > 0.05). Quantitative data with a normal distribution were analyzed with parametric tests, while the nonparametric test was used for data without a normal distribution. The difference between Pearson's correlation coefficient (PCC) for the colocalization of hFANCG-EGFP or truncated hFANCG-EGFP and MitoTracker in HeLa cells was evaluated with a parametric Brown-Forsythe and Welch analysis of variance (ANOVA) tests. A two-way ANOVA was used to compare the iron association with FANCG in wild-type, R22P, and FANCG KO fibroblast cells using cell type and incubation time as factors. Dunnett's test was used to perform multiple comparisons of iron association with FANCG under different incubation periods: wild-type fibroblast cells were taken as a control for each incubation time. The expressivity of iron metabolism genes (FXN and NFU1) in fibroblast cells (FG wild type/corrected and FGR22P) was evaluated using unpaired *t* tests. FG corrected fibroblast cells were taken as a control for each incubation time, and the Holm-Sidak method was used to analyze the expressivity of iron metabolism genes in FGR22P fibroblast cells without assuming a consistent SD. Similar unpaired *t* tests were used to analyze the PCC value for the colocalization of hTOM70-EGFP and MitoTracker in FGR22P fibroblast cells, except the SD was assumed the same because Levene's test for variation supported the null hypothesis of the same variation in this case. A *P* value of <0.05 was considered statistically significant.

SUPPLEMENTAL MATERIAL

Supplemental material is available online only.

SUPPLEMENTAL FILE 1, PDF file, 1.2 MB.

ACKNOWLEDGMENTS

We thank Agata Smogorzewska for providing the FA cell lines. We thank Jeffrey M. Rosen, Giovanni Pagano, K. Aikat, and A. Bhattacharya for critical reading of the manuscript.

This work was supported by the Department of Biotechnology (BT/PR1918/BRB/10/948/2011), Government of India. NIT Durgapur supported the fellowship to J.C.B.K. and B.S.K. We are thankful to DST-FIST for the instrument grant to the Department of Biotechnology, NIT Durgapur.

This work does not have any financial conflict of interest.

J.C.B.K. and B.S.K. performed the experiments. K.M. and S.G. studied the FA mutations. R.B.M. and S.K.M. helped the iron uptake experiment. S.S.M. planned the project and wrote the manuscript.

REFERENCES

- Nowell PC. 1976. The clonal evolution of tumor cell populations. *Science* 194:23–28. <https://doi.org/10.1126/science.959840>.
- Philpott CC, Rashford J, Yamaguchi-Iwai Y, Rouault TA, Dancis A, Klausner RD. 1998. Cell-cycle arrest and inhibition of G1 cyclin translation by iron in AFT1-1(up) yeast. *EMBO J* 17:5026–5036. <https://doi.org/10.1093/emboj/17.17.5026>.
- Veatch JR, McMurray MA, Nelson ZW, Gottschling DE. 2009. Mitochondrial dysfunction leads to nuclear genome instability via an iron-sulfur cluster defect. *Cell* 137:1247–1258. <https://doi.org/10.1016/j.cell.2009.04.014>.
- Kujoth GC, Hiona A, Pugh TD, Someya S, Panzer K, Wohlgemuth SE, Hofer T, Seo AY, Sullivan R, Jobling WA, Morrow JD, Van Remmen H, Sedivy JM, Yamasoba T, Tanokura M, Weindruch R, Leeuwenburgh C, Prolla TA. 2005. Mitochondrial DNA mutations, oxidative stress, and apoptosis in mammalian aging. *Science* 309:481–484. <https://doi.org/10.1126/science.1112125>.
- Vives-Bauza C, Gonzalo R, Manfredi G, Garcia-Arumi E, Andreu AL. 2006. Enhanced ROS production and antioxidant defenses in cybrids harbouring mutations in mtDNA. *Neurosci Lett* 391:136–141. <https://doi.org/10.1016/j.neulet.2005.08.049>.
- Kim GJ, Chandrasekaran K, Morgan WF. 2006. Mitochondrial dysfunction, persistently elevated levels of reactive oxygen species and radiation-induced genomic instability: a review. *Mutagenesis* 21:361–367. <https://doi.org/10.1093/mutage/gel048>.
- Yoshida T, Goto S, Kawakatsu M, Urata Y, Li TS. 2012. Mitochondrial dysfunction, a probable cause of persistent oxidative stress after exposure to ionizing radiation. *Free Radic Res* 46:147–153. <https://doi.org/10.3109/10715762.2011.645207>.
- Flury F, Von Borstel RC, Williamson DH. 1976. Mutator activity of petite strains of *Saccharomyces cerevisiae*. *Genetics* 83:645–653.
- Ichim G, Lopez J, Ahmed SU, Muthalagu N, Giampazolias E, Delgado ME, Haller M, Riley JS, Mason SM, Athineos D, Parsons MJ, van de Kooij B, Bouchier-Hayes L, Chalmers AJ, Rooswinkler RW, Oberst A, Blyth K, Rehm M, Murphy DJ, Tait SWG. 2015. Limited mitochondrial permeabilization causes DNA damage and genomic instability in the absence of cell death. *Mol Cell* 57:860–872. <https://doi.org/10.1016/j.molcel.2015.01.018>.
- Kumimoto H, Yamane Y, Nishimoto Y, Fukami H, Shinoda M, Hatoaka S, Ishizaki K. 2004. Frequent somatic mutations of mitochondrial DNA in esophageal squamous cell carcinoma. *Int J Cancer* 108:228–231. <https://doi.org/10.1002/ijc.11564>.
- Larman TC, DePalma SR, Hadjipanayis AG, Protopopov A, Zhang J, Gabriel SB, Chin L, Seidman CE, Kucherlapati R, Seidman JG, The Cancer Genome Atlas Research Network. 2012. Spectrum of somatic mitochondrial mutations in five cancers. *Proc Natl Acad Sci U S A* 109:14087–14091. <https://doi.org/10.1073/pnas.1211502109>.
- McMahon S, Laframboise T. 2014. Mutational patterns in the breast cancer mitochondrial genome, with clinical correlates. *Carcinogenesis* 35:1046–1054. <https://doi.org/10.1093/carcin/bgu012>.
- Kispal G, Csere P, Prohl C, Lill R. 1999. The mitochondrial proteins Atm1p and Nfs1p are essential for biogenesis of cytosolic Fe/S proteins. *EMBO J* 18:3981–3989. <https://doi.org/10.1093/emboj/18.14.3981>.
- Rosenberg PS, Socié G, Alter BP, Gluckman E. 2005. Risk of head and neck squamous cell cancer and death in patients with Fanconi anemia who did and did not receive transplants. *Blood* 105:67–73. <https://doi.org/10.1182/blood-2004-04-1652>.
- Bluteau D, Masliah-Planchon J, Clairmont C, Rousseau A, Ceccaldi R, Dubois d'Enghien C, Bluteau O, Cuccuini W, Gachet S, Peffault de Latour R, Leblanc T, Socié G, Baruchel A, Stoppa-Lyonnet D, D'Andrea AD, Soulier J. 2016. Biallelic inactivation of REV7 is associated with Fanconi anemia. *J Clin Invest* 126:3580–3584. <https://doi.org/10.1172/JCI88010>.
- Walden H, Deans AJ. 2014. The Fanconi anemia DNA repair pathway: structural and functional insights into a complex disorder. *Annu Rev Biophys* 43:257–278. <https://doi.org/10.1146/annurev-biophys-051013-022737>.
- Guo M, Vidhyasagar V, Ding H, Wu Y. 2014. Insight into the roles of helicase motif Ia by characterizing Fanconi anemia group J protein (FANCI) patient mutations. *J Biol Chem* 289:10551–10565. <https://doi.org/10.1074/jbc.M113.538892>.
- Rudolf J, Makrantonis V, Ingledew WJ, Stark MJR, White MF. 2006. The DNA repair helicases XPD and FancJ have essential iron-sulfur domains. *Mol Cell* 23:801–808. <https://doi.org/10.1016/j.molcel.2006.07.019>.
- Guo M, Vidhyasagar V, Talwar T, Kariem A, Wu Y. 2016. Mutational analysis of FANCI helicase. *Methods* 108:118–129. <https://doi.org/10.1016/j.ymeth.2016.04.023>.
- Wu Y, Sommers JA, Suhasini AN, Leonard T, Deakyne JS, Mazin AV, Shin-Ya K, Kitao H, Brosh RM. 2010. Fanconi anemia group J mutation abolishes its DNA repair function by uncoupling DNA translocation from helicase activity or disruption of protein-DNA complexes. *Blood* 116:3780–3791. <https://doi.org/10.1182/blood-2009-11-256016>.
- Brosh RM, Cantor SB. 2014. Molecular and cellular functions of the FANCI DNA helicase defective in cancer and in Fanconi anemia. *Front Genet* 5:32.
- Mukhopadhyay SS, Leung KS, Hicks MJ, Hastings PJ, Youssoufian H, Plon SE. 2006. Defective mitochondrial peroxiredoxin-3 results in sensitivity to oxidative stress in Fanconi anemia. *J Cell Biol* 175:225–235. <https://doi.org/10.1083/jcb.200607061>.
- Pagano G, Shyamsunder P, Verma RS, Lyakhovich A. 2014. Damaged mitochondria in Fanconi anemia—an isolated event or a general phenomenon? *Oncoscience* 1:287–295. <https://doi.org/10.18632/oncoscience.29>.
- Zhang T, Du W, Wilson AF, Namekawa SH, Andreassen PR, Meetei AR, Pang Q. 2017. Fancd2 in vivo interaction network reveals a non-canonical role in mitochondrial function. *Sci Rep* 7:45626. <https://doi.org/10.1038/srep45626>.
- Backes S, Hess S, Boos F, Woellhaf MW, Gödel S, Jung M, Mühlhaus T, Herrmann JM. 2018. Tom70 enhances mitochondrial preprotein import efficiency by binding to internal targeting sequences. *J Cell Biol* 217:1369–1382. <https://doi.org/10.1083/jcb.201708044>.
- Nickel C, Horneff R, Heermann R, Neumann B, Jung K, Soll J, Schwenkert S. 2019. Phosphorylation of the outer membrane mitochondrial protein OM64 influences protein import into mitochondria. *Mitochondrion* 44:93–102. <https://doi.org/10.1016/j.mito.2018.01.005>.
- Wilson JB, Blom E, Cunningham R, Xiao Y, Kupfer GM, Jones NJ. 2010. Several tetratricopeptide repeat (TPR) motifs of FANCG are required for assembly of the BRCA2/D1-D2-G-X3 complex, FANCD2 monoubiquitylation and phleomycin resistance. *Mutat Res* 689:12–20. <https://doi.org/10.1016/j.mrfmmm.2010.04.003>.
- Bannai H, Tamada Y, Maruyama O, Nakai K, Miyano S. 2002. Extensive feature detection of N-terminal protein sorting signals. *Bioinformatics* 18:298–305. <https://doi.org/10.1093/bioinformatics/18.2.298>.
- Qiao F, Mi J, Wilson JB, Zhi G, Bucheimer NR, Jones NJ, Kupfer GM. 2004. Phosphorylation of Fanconi anemia (FA) complementation group G protein, FANCG, at serine 7 is important for function of the FA pathway. *J Biol Chem* 279:46035–46045. <https://doi.org/10.1074/jbc.M408323200>.
- Wilson JB, Yamamoto K, Marriott AS, Hussain S, Sung P, Hoatlin ME, Mathew CG, Takata M, Thompson LH, Kupfer GM, Jones NJ. 2008. FANCG promotes formation of a newly identified protein complex containing BRCA2, FANCD2 and XRCC3. *Oncogene* 27:3641–3652. <https://doi.org/10.1038/sj.onc.1211034>.
- Auerbach AD, Greenbaum J, Pujara K, Batish SD, Bitencourt MA, Koke-mohr I, Schneider H, Lobitz S, Pasquini R, Giampietro PF, Hanenberg H, Levan O, International Fanconi Anemia Registry. 2003. Spectrum of sequence variation in the FANCG gene: an International Fanconi Anemia Registry (IFAR) study. *Hum Mutat* 21:158–168. <https://doi.org/10.1002/humu.10166>.
- Tokarz P, Blasiak J. 2014. Role of mitochondria in carcinogenesis. *Acta Biochim Pol* 61. https://doi.org/10.18388/abp.2014_1829.
- Kaniak-Golik A, Skoneczna A. 2015. Mitochondria-nucleus network for genome stability. *Free Radic Biol Med* 82:73–104. <https://doi.org/10.1016/j.freeradbiomed.2015.01.013>.

34. Richardson DR, Lane DJR, Becker EM, Huang ML-H, Whitnall M, Rahmanto YS, Sheftel AD, Ponka P. 2010. Mitochondrial iron trafficking and the integration of iron metabolism between the mitochondrion and cytosol. *Proc Natl Acad Sci U S A* 107:10775–10782. <https://doi.org/10.1073/pnas.0912925107>.
35. Lill R, Hoffmann B, Molik S, Pierik AJ, Rietzschel N, Stehling O, Uzarska MA, Weibert H, Wilbrecht C, Mühlenhoff U. 2012. The role of mitochondria in cellular iron-sulfur protein biogenesis and iron metabolism. *Biochim Biophys Acta* 1823:1491–1508. <https://doi.org/10.1016/j.bbamcr.2012.05.009>.
36. Wu Y, Brosh R, Jr. 2009. FANCF helicase operates in the Fanconi anemia DNA repair pathway and the response to replicational stress. *Curr Mol Med* 9:470–482. <https://doi.org/10.2174/156652409788167159>.
37. Pierik AJ, Netz DJA, Lill R. 2009. Analysis of iron-sulfur protein maturation in eukaryotes. *Nat Protoc* 4:753–766. <https://doi.org/10.1038/nprot.2009.39>.
38. Mackenzie EL, Iwasaki K, Tsuji Y. 2008. Intracellular iron transport and storage: from molecular mechanisms to health implications. *Antioxidants Redox Signal* 10:997–1030. <https://doi.org/10.1089/ars.2007.1893>.
39. Lill R, Mühlenhoff U. 2008. Maturation of iron-sulfur proteins in eukaryotes: mechanisms, connected processes, and diseases. *Annu Rev Biochem* 77:669–700. <https://doi.org/10.1146/annurev.biochem.76.052705.162653>.
40. Schendzielorz AB, Schulz C, Lytovchenko O, Clancy A, Guiard B, Ieva R, van der Laan M, Rehling P. 2017. Two distinct membrane potential-dependent steps drive mitochondrial matrix protein translocation. *J Cell Biol* 216:83–92. <https://doi.org/10.1083/jcb.201607066>.
41. Ahting U, Waizenegger T, Neupert W, Rapaport D. 2005. Signal-anchored proteins follow a unique insertion pathway into the outer membrane of mitochondria. *J Biol Chem* 280:48–53. <https://doi.org/10.1074/jbc.M410905200>.
42. Parmar K, D'Andrea A, Niedernhofer LJ. 2009. Mouse models of Fanconi anemia. *Mutat Res* 668:133–140. <https://doi.org/10.1016/j.mrfmmm.2009.03.015>.
43. Pulliam-Leath AC, Ciccone SL, Nalepa G, Li X, Si Y, Miravalle L, Smith D, Yuan J, Li J, Anur P, Orazi A, Vance GH, Yang FC, Hanenberg H, Bagby GC, Clapp DW. 2010. Genetic disruption of both Fancc and Fancg in mice recapitulates the hematopoietic manifestations of Fanconi anemia. *Blood* 116:2915–2920. <https://doi.org/10.1182/blood-2009-08-240747>.
44. Yang Y, Kuang Y, Montes De Oca R, Hays T, Moreau L, Lu N, Seed B, D'Andrea AD. 2001. Targeted disruption of the murine Fanconi anemia gene, Fancg/Xrcc9. *Blood* 98:3435–3440. <https://doi.org/10.1182/blood.v98.12.3435>.
45. Neve EP, Ingelman-Sundberg M. 2001. Identification and characterization of a mitochondrial targeting signal in rat cytochrome P450 2E1 (CYP2E1). *J Biol Chem* 276:11317–11322. <https://doi.org/10.1074/jbc.M008640200>.
46. Nunnari J, Suomalainen A. 2012. Mitochondria: in sickness and in health. *Cell* 148:1145–1159. <https://doi.org/10.1016/j.cell.2012.02.035>.
47. Netz DJA, Mascarenhas J, Stehling O, Pierik AJ, Lill R. 2014. Maturation of cytosolic and nuclear iron-sulfur proteins. *Trends Cell Biol* 24:303–312. <https://doi.org/10.1016/j.tcb.2013.11.005>.
48. Biederbick A, Stehling O, Rosser R, Niggemeyer B, Nakai Y, Elsasser H-P, Lill R. 2006. Role of human mitochondrial Nfs1 in cytosolic iron-sulfur protein biogenesis and iron regulation. *Mol Cell Biol* 26:5675–5687. <https://doi.org/10.1128/MCB.00112-06>.
49. Odermatt DC, Lee WTC, Wild S, Jozwiakowski SK, Rothenberg E, Gari K. 2020. Cancer-associated mutations in the iron-sulfur domain of FANCF affect G-quadruplex metabolism. *PLoS Genet* 16:e1008740. <https://doi.org/10.1371/journal.pgen.1008740>.
50. Li K, Singh A, Crooks DR, Dai X, Cong Z, Pan L, Ha D, Rouault TA. 2010. Expression of human frataxin is regulated by transcription factors SRF and TFAP2. *PLoS One* 5:e12286. <https://doi.org/10.1371/journal.pone.0012286>.
51. Wang Y-T, Chuang J-Y, Shen M-R, Yang W-B, Chang W-C, Hung J-J. 2008. Sumoylation of specificity protein 1 augments its degradation by changing the localization and increasing the specificity protein 1 proteolytic process. *J Mol Biol* 380:869–885. <https://doi.org/10.1016/j.jmb.2008.05.043>.
52. Dunn KW, Kamocka MM, McDonald JH. 2011. A practical guide to evaluating colocalization in biological microscopy. *Am J Physiol Cell Physiol* 300:C723–C742. <https://doi.org/10.1152/ajpcell.00462.2010>.
53. Rouault TA. 2012. Biogenesis of iron-sulfur clusters in mammalian cells: new insights and relevance to human disease. *Dis Model Mech* 5:155–164. <https://doi.org/10.1242/dmm.009019>.